



# **UNIVERSIDAD DE INVESTIGACIÓN DE TECNOLOGÍA EXPERIMENTAL YACHAY**

**Escuela de Ciencias Físicas y Nanotecnología**

**TÍTULO: The optical properties of Diatoms doped with Plasmonic  
Nanoparticles for Biomedical Applications**

Trabajo de integración curricular presentado como requisito para la  
obtención del título de Ingeniero en Nanotecnología

**Autor:**

Adrián Javier León Valencia

**Tutor:**

PhD. Gema González

**Co - Tutor:**

PhD. Sarah Briceño

Urcuquí, junio 2021

Urcuquí, 11 de junio de 2021

**SECRETARÍA GENERAL**  
**(Vicerrectorado Académico/Cancillería)**  
**ESCUELA DE CIENCIAS FÍSICAS Y NANOTECNOLOGÍA**  
**CARRERA DE NANOTECNOLOGÍA**  
**ACTA DE DEFENSA No. UITEY-PHY-2021-00012-AD**

A los 11 días del mes de junio de 2021, a las 12:00 horas, de manera virtual mediante videoconferencia, y ante el Tribunal Calificador, integrado por los docentes:

<b>Presidente Tribunal de Defensa</b>	Dr. REINOSO CARLOS , Ph.D.
<b>Miembro No Tutor</b>	Dr. CHACON TORRES, JULIO CESAR , Ph.D.
<b>Tutor</b>	Dra. GONZALEZ VAZQUEZ, GEMA , Ph.D.

El(la) señor(ita) estudiante **LEON VALENCIA, ADRIAN JAVIER**, con cédula de identidad No. **1752981538**, de la **ESCUELA DE CIENCIAS FÍSICAS Y NANOTECNOLOGÍA**, de la Carrera de **NANOTECNOLOGÍA**, aprobada por el Consejo de Educación Superior (CES), mediante Resolución **RPC-SO-13-No.156-2015**, realiza a través de videoconferencia, la sustentación de su trabajo de titulación denominado: **The optical properties of Diatoms doped with Plasmonic nanoparticles for Biomedical Applications**, previa a la obtención del título de **INGENIERO/A EN NANOTECNOLOGÍA**.

El citado trabajo de titulación, fue debidamente aprobado por el(los) docente(s):

<b>Tutor</b>	Dra. GONZALEZ VAZQUEZ, GEMA , Ph.D.
<b>Co - Tutor</b>	Dra. BRICEÑO ARAUJO, SARAH ELISA , Ph.D.

Y recibió las observaciones de los otros miembros del Tribunal Calificador, las mismas que han sido incorporadas por el(la) estudiante.

Previamente cumplidos los requisitos legales y reglamentarios, el trabajo de titulación fue sustentado por el(la) estudiante y examinado por los miembros del Tribunal Calificador. Escuchada la sustentación del trabajo de titulación a través de videoconferencia, que integró la exposición de el(la) estudiante sobre el contenido de la misma y las preguntas formuladas por los miembros del Tribunal, se califica la sustentación del trabajo de titulación con las siguientes calificaciones:

Tipo	Docente	Calificación
Presidente Tribunal De Defensa	Dr. REINOSO CARLOS , Ph.D.	9,8
Miembro Tribunal De Defensa	Dr. CHACON TORRES, JULIO CESAR , Ph.D.	10,0
Tutor	Dra. GONZALEZ VAZQUEZ, GEMA , Ph.D.	10,0

Lo que da un promedio de: **9.9 (Nueve punto Nueve)**, sobre 10 (diez), equivalente a: **APROBADO**

Para constancia de lo actuado, firman los miembros del Tribunal Calificador, el/la estudiante y el/la secretario ad-hoc.

*Certifico que en cumplimiento del Decreto Ejecutivo 1017 de 16 de marzo de 2020, la defensa de trabajo de titulación (o examen de grado modalidad teórico práctica) se realizó vía virtual, por lo que las firmas de los miembros del Tribunal de Defensa de Grado, constan en forma digital.*

**LEON VALENCIA, ADRIAN JAVIER**  
**Estudiante**

**Dr. REINOSO CARLOS , Ph.D.**  
**Presidente Tribunal de Defensa**

Digitally signed by CARLOS ALBERTO  
 REINOSO JÉREZ  
 Date: 2021.06.11 14:06:15 COT

Dra. GONZALEZ VAZQUEZ, GEMA , Ph.D.  
**Tutor**



Firmado electrónicamente por:  
**GEMA  
GONZALEZ**

Dr. CHACON TORRES, JULIO CESAR , Ph.D.  
**Miembro No Tutor**



Firmado electrónicamente por:  
**JULIO CESAR  
CHACON TORRES**

CIFUENTES TAFUR, EVELYN CAROLINA  
**Secretario Ad-hoc**



Firmado electrónicamente por:  
**EVELYN CAROLINA  
CIFUENTES TAFUR**

## **AUTORÍA**

Yo, **ADRIAN JAVIER LEON VALENCIA**, con cédula de identidad 1752981538, declaro que las ideas, juicios, valoraciones, interpretaciones, consultas bibliográficas, definiciones y conceptualizaciones expuestas en el presente trabajo; así cómo, los procedimientos y herramientas utilizadas en la investigación, son de absoluta responsabilidad de el/la autora (a) del trabajo de integración curricular. Así mismo, me acojo a los reglamentos internos de la Universidad de Investigación de Tecnología Experimental Yachay.

Urcuquí, junio 2021.



---

Adrián Javier León Valencia  
CI: 1752981538

## AUTORIZACIÓN DE PUBLICACIÓN

Yo, **ADRIÁN JAVIER LEÓN VALENCIA**, con cédula de identidad 1752981538, cedo a la Universidad de Tecnología Experimental Yachay, los derechos de publicación de la presente obra, sin que deba haber un reconocimiento económico por este concepto. Declaro además que el texto del presente trabajo de titulación no podrá ser cedido a ninguna empresa editorial para su publicación u otros fines, sin contar previamente con la autorización escrita de la Universidad.

Asimismo, autorizo a la Universidad que realice la digitalización y publicación de este trabajo de integración curricular en el repositorio virtual, de conformidad a lo dispuesto en el Art. 144 de la Ley Orgánica de Educación Superior

Urcuquí, junio 2021.



---

Adrián Javier León Valencia  
CI: 1752981538

## **Dedication**

To my parents, who supported me along the way and on each step I took. For the trips back and forth to the university, and the support for my high aspirations in life.

To my brother and sister for their cozy welcome each time and for cheering me up with their laughs. For all this energy that filled me up each week. Thank you all!

## **Acknowledgements**

The full process would not have been possible without the patience from both my advisor Gema González and coadvisor Sarah Briceño. Special thanks to professors who helped me along the process and dedicated their times even during this pandemic period. Finally, but not less important, I would to thank my parents and full family for the support and motivation along the process since this would have been impossible without their push. Yachay has become an important part of my journey in this life and will always remain deep in my heart.

## **Resumen**

Las diatomeas son un ser vivo abundante a lo largo del planeta, de las cuales, sus estructuras externas son quasi-simétricas y representan una base ideal para posterior funcionalización y decoración con nanopartículas plasmónicas. Este estudio realiza un análisis extensivo, donde la longitud de onda de la luz es probada como un agente reductor durante el proceso de síntesis in-situ de nanopartículas de oro y de plata. Diferentes tiempos de exposición y un agente reductor adicional son usados para comparar la eficiencia y efectos de los distintos tamaños y formas de las nanopartículas. Finalmente, análisis comparativos fueron desarrollados antes y después de añadir ADN, con técnicas como fluorescencia y espectroscopia raman, a las frústulas decoradas con el fin de probar su habilidad como biosensores. A partir de estos resultados, decoración con nanopartículas de plata funciona de mejor manera como sensor para señales raman, mientras que decoración con nanopartículas de oro funciona mejor bajo microscopía de fluorescencia.

**Palabras clave:** Diatomeas, frústulas, sensor, biosensor, nanopartículas, efecto de luz.

## **Abstract**

Diatoms are an abundant living being along the planet, from which their outer structures are quasi symmetrical and thus represent an ideal template for further functionalisation and plasmonic decoration. This study performs an extensive analysis where light wavelength is tested as reductor agent during the in-situ synthesis process of both Gold and Silver nanoparticles. Different exposure times and an additional reductor agent are used to compare the efficiency and effects of nanoparticles sizes and shapes. Finally, comparative analysis were developed before and after DNA attachment, with fluorescence and raman spectroscopy techniques, to decorated frustules in order to test viability as biosensors. From here, Silver decoration seems to work the best for sensing under raman signals, while Gold decoration under fluorescence microscopy.

**Keywords:** Diatoms, frustules, sensor, biosensor, nanoparticles, light effect.

# Contents

<b>List of Figures</b>	<b>xi</b>
<b>List of Tables</b>	<b>xiv</b>
<b>1 Introduction</b>	<b>1</b>
1.0.1 Current approaches . . . . .	2
1.1 Motivation . . . . .	3
1.2 Problem Statement . . . . .	3
1.3 General and Specific Objectives . . . . .	4
1.3.1 General Objective . . . . .	4
1.3.2 Specific Objectives . . . . .	4
<b>2 Theoretical Background</b>	<b>5</b>
2.0.1 Nanotechnology . . . . .	5
2.0.2 Nanomaterials . . . . .	6
2.0.3 Bioimaging . . . . .	6
2.0.4 Biosensors . . . . .	6
2.0.5 Photoluminescence . . . . .	7
2.0.6 Diatoms . . . . .	8
2.0.7 Plasmonic nanoparticles . . . . .	10
2.0.8 Diatoms doped with Luminescent Elements . . . . .	13
2.0.9 State of the Art . . . . .	13
2.1 Characterization Techniques . . . . .	14

2.1.1	Raman Spectroscopy . . . . .	14
2.1.2	Ultraviolet-visible Spectroscopy (UV-Vis) . . . . .	17
2.1.3	Scanning Electron Microscopy (SEM) . . . . .	19
2.1.4	Scanning Transmission Electron Microscopy (STEM) mode in SEM . . . . .	20
2.1.5	Photo-luminescence Excitation (PLE) . . . . .	21
2.1.6	Fourier Transform Infrared . . . . .	23
<b>3</b>	<b>Methodology</b>	<b>27</b>
3.1	Chemicals . . . . .	27
3.2	Light Chambers . . . . .	27
3.3	Synthesis . . . . .	28
3.3.1	Diatoms extraction . . . . .	28
3.3.2	Ag/Au Reduction and deposition on Diatoms . . . . .	29
3.3.3	DNA extraction and attachment to diatoms . . . . .	31
3.4	Characterization Equipment . . . . .	33
3.4.1	UV-Vis Spectroscopy . . . . .	33
3.4.2	Raman Spectroscopy . . . . .	34
3.4.3	Scanning Electron Microscopy (SEM) . . . . .	35
3.4.4	Scanning Transmission Electron Microscopy (STEM) . . . . .	37
3.4.5	Fluorescence Microscopy . . . . .	38
3.4.6	Fourier Transform Infrared spectroscopy . . . . .	39
<b>4</b>	<b>Results &amp; Discussion</b>	<b>41</b>
4.1	Diatoms decoration process . . . . .	41
4.1.1	Diatoms cleaning . . . . .	41
4.1.2	Diatoms surface decoration Au/Ag Nanoparticles . . . . .	41
4.1.3	Decorated Diatoms - DNA attachment . . . . .	42
4.2	Characterization Au/Ag Nanoparticles . . . . .	42
4.2.1	UV-Vis Spectroscopy . . . . .	42
4.2.2	Scanning Electron Microscopy (SEM) . . . . .	46
4.2.3	Scanning Transmission Electron Microscopy (STEM) . . . . .	48

4.2.4	Raman Spectroscopy . . . . .	50
4.2.5	Fluorescence Microscopy . . . . .	54
4.2.6	Fourier Transform Infrared Spectroscopy (FTIR) . . . . .	56
<b>5</b>	<b>Conclusions &amp; Outlook</b>	<b>59</b>
<b>A</b>	<b>Short Appendix 1 Heading for the Table of Contents</b>	<b>61</b>
	<b>Bibliography</b>	<b>69</b>

# List of Figures

2.1	Photoluminescence scheme showing internal energy transitions. . . . .	7
2.2	Various shapes and morphology of diatoms in water sources. . . . .	9
2.3	TEM/SEM example images of Silver Nanoparticles. . . . .	11
2.4	Gold Nanoparticles shapes review with their respective synthesis method. . . . .	12
2.5	Main energy transitions captured by Raman Spectroscopy. . . . .	15
2.6	Raman Spectroscopy working principle and components. . . . .	16
2.7	LSPR basic principle for increased raman signal. . . . .	17
2.8	UV-Vis working principle to capture absorbance. . . . .	18
2.9	Scheme of SEM imaging technique with its components. . . . .	19
2.10	Light path and set up STEM mode in SEM . . . . .	20
2.11	Fluorescence microscopy working principle and path of light towards the detector. . . . .	22
2.12	FTIR equipment and working principle. . . . .	23
3.1	Light chambers disposition for two different wavelengths excitation. . . . .	28
3.2	Diatoms extractions source: sedimentary rock. . . . .	29
3.3	Decorated diatoms after 4h exposure to light source. . . . .	30
3.4	Decorated diatoms after 2 hours of light exposure. . . . .	31
3.5	UV-Vis spectroscopy equipment for absorption spectra analysis, along with most relevant peaks. . . . .	34
3.6	Raman Spectroscopy analysis equipment and most relevant diatom and nanoparticles spectra. . . . .	35
3.7	SEM micrography acquisition equipment and image from Aulacoseira diatom group. . . . .	36
3.8	STEM sample image of Ag and Au nanoparticles . . . . .	37
3.9	Microscope used in fluorescence imaging mode with example image. . . . .	39

3.10	FTIR equipment at the solid sample mode, along with example spectra of DNA and frustules. . . . .	40
4.1	UV-Vis spectra from diatoms doped with Au nanoparticles growth under blue light exposure. . . . .	43
4.2	UV-Vis spectra from diatoms doped with Ag nanoparticles growth under blue light exposure. . . . .	44
4.3	UV-Vis spectra from diatoms doped with Au nanoparticles. Borohydride addition (G2). . . . .	44
4.4	UV-Vis spectra from diatoms doped with Ag nanoparticles. Borohydride addition (G2). . . . .	45
4.5	SEM comparing Au NPs of G1 and G2 after 4h exposure to green light. . . . .	46
4.6	SEM decorated diatoms with Au NPs G2 after 4h of blue and green light exposure. . . . .	50
4.7	SEM decorated diatoms with Ag NPs G2 after 4h of blue and green light exposure. . . . .	51
4.8	Raman spectra of Ag NPs on diatoms with DNA attached. . . . .	53
4.9	Raman spectra at two excitation wavelengths, Ag NPs 4h exposure, after DNA attachment. . . . .	54
4.10	Fluorescence microscopy mode for Au NPs decorated diatoms from G2 at 4h exposure to blue light. Before and after DNA attachment . . . . .	55
4.11	FTIR spectra of diatoms before and after Au NPs decoration, along with DNA. . . . .	58
4.12	FTIR spectra of diatoms before and after Ag NPs decoration, along with DNA. . . . .	58
A.1	Raman spectra of Au NPs before and after DNA attachment. . . . .	63
A.2	STEM images for G1 Au NPs used to calculate average nanoparticles sizes. . . . .	64
A.3	STEM images for G1 Ag NPs used to calculate average nanoparticles size. . . . .	65
A.4	STEM images for G2 Au NPs used to calculate average nanoparticles size. . . . .	66
A.5	STEM images for G2 Ag NPs used to calculate average nanoparticles size. . . . .	67

# List of Tables

2.1	FTIR referential peaks to molecular compounds assignment. . . . .	25
4.1	Main UV-Vis peaks obtained for Ag/Au nanoparticles on diatoms. . . . .	45
4.2	Nanoparticles average sizes obtained from STEM images for G1 and G2 groups. . . . .	48

# Chapter 1

## Introduction

During the last years, research concerning nanomaterials and their biomedical application have hugely increased. Even more, research and economical investment in the field of nanotechnology has kept a constant increase rate, mainly in first world countries such as South Korea, which is leading the rank of "research and development expenditure" by the year 2018, according to The World Bank data.

Biomaterials and more specifically biological nanomaterials have gained space in the field of biomedicine. A variety of synthesis methods, versatility and further increase of their features by doping of the materials, has turned them in the focus of the next generation of biomedical tools. Applications within this field range between drug delivery purposes, carriers, target-specific nanomaterials, to even sensors, bioimaging materials or tools for cancer treatment. However, to meet these purposes, some requirements need to be fulfilled beforehand, being biocompatibility one of the main ones.

In matters of biosensing and bioimaging materials, diatoms have shown to be a great option due to their particular structure, characteristic shapes, replicability, luminescent properties and biocompatibility. Additionally, the options for improvement is enormous since its surface might be decorated with different materials depending on the characteristic that is needed to be enhanced.

In particular, within this study, the luminescence property is observed and further increased by the use of plasmonic nanoparticles, such as Gold and Silver Nanoparticles. Furthermore, the reduction process is tested by the use

of different light sources, as well as with the addition of reducing agents.

The analysis here performed, represents the previous step of creating a functional biosensor taking advantage of the luminescence in diatom frustules and plasmonic nanoparticles. More precisely here it is shown how both emission and absorption in doped diatoms can be tuned. Further studies can be performed since parameters like shape and sizes of nanoparticles are not taken into account, and thus it leaves place for future research development.

### **1.0.1 Current approaches**

For a long while, diatoms have been known for its symmetrical structure and enormous surface area due to its porosity and hierarchical structure. Research concerning diatoms has significantly increased during the last decade due to the already mentioned properties. At the moment, a variety of functionalization process are explored in order to increase the number of features and functions to the frustules in diatoms. In function of the symmetry, two main classes might be assigned: centric diatoms and pennate diatoms, from which the first one is mainly planktonic with round or polygonal valves, whereas the latter is mainly benthonic with bipolar, elongated valves<sup>1</sup>.

Furthermore, due to the importance of eliminating carbon residues on the frustules, organic content and even to create spot on the surface for promoting nucleation, cleaning methods have been explored. By now, a piranha treatment, hydrogen peroxide or immersion in any acidic solution followed by rinsing and centrifugation is the usual cleaning method<sup>2</sup>. However, there are recent methods that might gain place since they are more environmentally friendly and cost-effective, with acceptable or even better performances in organic residues removal<sup>3</sup>.

Functionalization, thus, is the step to follow after cleaning. For this purpose, a variety of paths can be followed such as: Metabolic Doping,

Metalization for Application in Plasmonics, Functionalization for Protein Immobilization, Replicas or Genetic Modification, topics covered by Rogato and De Tomasi (2020)<sup>1</sup>.

Moreover, one of the properties of our interest is the luminescence since this characteristic might be easily manipulated for sensing or imaging purposes. Diatoms by themselves have non tunable luminescence peaks spectra and appearing at the UV range, hence frustule modification (doping) has become the main approach in the last years,

being one option the use of plasmonic nanoparticles. Theoretical research has shown that surface plasmon resonance corresponding to metallic nanoparticles significantly increase the luminescence on diatoms. Simulations predict stronger optical extinction and enhanced localized electric field, further confirmed by the use of SERS measurements with over 4 times improvement<sup>4</sup>.

Concerning specific applications of these materials, is the Surface Enhanced Raman Spectroscopy (SERS) due to the already mentioned enhancement of luminescent properties. However, also improvements in light transmission is observed by the use of this material, due to the periodic or quasi-periodic hole arrays present in diatoms<sup>5?</sup>. Extraordinary transmission effects (EOT), thus, could be ascribed for diatoms, finding applications in integrated optics and chemical biosensing<sup>1</sup>.

## 1.1 Motivation

Diatoms themselves have the advantage of being biocompatible, making them a great option for biomedical purposes. Moreover, they show interesting features in matters of morphology, luminescence, large surface area due to the porous structure, replicability and remarkable optical properties with numerous applications<sup>6,7</sup>, which after a proper cleaning, might also be decorated and hence enhancing its light emission process.

The motivation for this project comes mainly from the possibility of creating biosensors, due to the hierarchical and quasi symmetrical structure in diatoms. For which, the study of light as a reducing agent for both Silver and Gold Nanoparticles was performed, checked the deposition process performed over diatoms of the mentioned nanoparticles and finally test the luminescence enhancement of diatoms after doping with plasmonic nanoparticles along with DNA molecule.

## 1.2 Problem Statement

The need of using additional fluorescent molecules to produce a signal. However, in the case of diatoms, their structure itself is luminescent due to the components and natural design. This, removes the need of external molecules and reduces the cost for producing biosensors.

## **1.3 General and Specific Objectives**

### **1.3.1 General Objective**

Doping diatoms with different Plasmonic Nanoparticles (Au, Ag) for increasing the luminescence properties when an external agent is attached to its surface.

### **1.3.2 Specific Objectives**

- To synthesize plasmonic nanoparticles using an in-situ method in two different forms: with and without the addition of Borohydride to support the synthesis.
- To dope diatoms with plasmonic nanoparticles by coating their frustules during the in-situ synthesis process of the latter and constant stirring.
- To study the effect of blue and green light as a reductor agent into the nanoparticles growing process for various times exposure.
- To characterize by microscopy and spectroscopy techniques, for evaluating doped diatoms luminescence properties and their changes after the attachment of DNA molecules.

## Chapter 2

# Theoretical Background

Along this chapter, some concepts and definitions will be explained for having a better of the research developed. Besides, this will give an overview of the state of the art concerning diatoms, plasmonic nanoparticles and biosensors or further applications.

### 2.0.1 Nanotechnology

Nanotechnology is a constant growing field. Several different branches within this field emerge along the years, as well as the technological developments it promotes with the progress of research. In general, nanotechnology refers to the study of materials and devices within the range of the nanometer scale; this is between 0 and 100 nm<sup>8</sup>. Structures of biological and synthetic origin can be created and even taking nature itself as an example of wise architecture, creating nano-structures based on already existing materials along the planet<sup>9</sup>. Nanomaterials face a variety of challenges, from which toxicity for biomedical applications is of great concern along the scientific community<sup>10</sup>.

The term encapsulates an enormous variety of devices and materials, ranging in categories such as nanosensors, nanorobotics, nanoelectronics, nanomagnetism, nanolithography and nano biomimetic materials, among others. Since the categories are so numerous, the spectrum of application is even greater. Namely, biosensors for dental diagnosis, "*nano-toothbrush*" for preventive dentistry<sup>11</sup>, nanorobotics for nanoassembly<sup>12</sup>, nanomachines for cancer therapeutics or biomedical instrumentation surgery<sup>13</sup>.

## **2.0.2 Nanomaterials**

More specifically, nanomaterials studies focus on the properties displayed at the nanoscale, which might be physical or chemical. In the case of physical properties, size and shapes are very important, mainly classified as zero, one, two or three dimensional materials<sup>14</sup>. Surface effects such as larger surface area, charge and stability provide specific properties to the material, which might be lower melting points, higher reactivity at the surface or less stability<sup>15</sup>. Normally, in bulk materials the properties would be determined by the interior atoms, however in the case of nanomaterials, the surface will define the features due to a larger surface area<sup>16</sup>. At this range, where the size of the particle is comparable to the wavelength of the electron, quantum effects are more relevant and thus quantum confinement has a stronger influence on the description of the material. Quantum confinement intends to describe any nanomaterial in terms of its energy levels, potential wells, valence and conduction bands, and band gaps<sup>17</sup>

## **2.0.3 Bioimaging**

Several techniques are currently being used for imaging purposes. Most of these techniques require certain contrast agent for better image acquisition. The nanoparticles used for these purposes need to fulfil specific features such as: high sensitivity, specificity, biocompatibility, as well as high luminescence for contrast purposes (<sup>18</sup>). The property of diatom and specifically, their frustules of forming photonic crystals, allow the possible of further use with bioimaging purposes or for contrast enhancement as proposed by Li (2011)<sup>19</sup>. This will not be assessed during the study, however it is included into the wide range of possible applications of diatom frustules

## **2.0.4 Biosensors**

Biosensors is a term widely used in the last century and comes in hand since the words biology and sensors have been merged in science. The term of biosensor refers to a chemical sensor that transform chemical information into a digital signal or something we can measure. Besides, there are two main components working together, which are the chemical recognition system and followed by the psycho-chemical transducer<sup>20</sup>.

A variety of different biosensors are now available on the market and serve for many different purposes, as well as they are made of different structures and additional components to improve their performance. The term is adopted within this research, mostly due to the photoluminescence of the material, which would allow to detect

when a specific molecule attaches to Diatoms decorated with plasmonic nanoparticles.

## 2.0.5 Photoluminescence

Photoluminescence (PL) principles are governed by electronic transitions. The photoluminescent process takes place in semiconductors, when they are on its way back to the ground state after an electron has been excited. Thus, they decrease their energy by releasing a photon which is measurable and appears on techniques such as PL spectra or PL quantum efficiency (PLQE)<sup>21</sup>, as shown in Fig.2.1. This term is used to describe two different types of luminescent processes, which are fluorescence and phosphorescence.

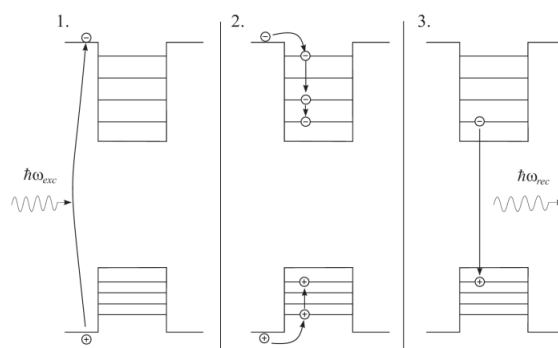


Figure 2.1: PLE scheme showing the initial excitation with a photon, then creating an electron-hole pair (1), relaxation process (2) and the final recombination (3), releasing energy in form of a photon. Adapted from<sup>22</sup>.

At the middle of Fig. 2.1, the relaxation processes is observed, where the electron at the Valence band goes to lower energy levels by releasing energy like photons. Finally, the right side of the figure shows the recombination process between electron-hole pair and releasing energy in form of a photon. However, there are porous structures that might as well diffract the light and produce this photoluminescence effect. One clear example of this is porous Si and thus diatoms, which has attracted attention since it might serve for various biomedical purposes, namely: as biosensor or as a bioimaging material due to its luminescent properties<sup>23</sup>.

## Fluorescence

Since fluorescence is one of the two types of luminescence processes explained above, it follows the same working principle. Released energy in forms of photons, usually has a longer wavelength than the absorption energy, which is called the Stokes shift<sup>24</sup>. This is due to the transitions occurred before the release of the photon and in contrast with phosphorescence, it disappears when the source of light is removed<sup>25</sup>.

### 2.0.6 Diatoms

Diatoms are a silica based material, which are the main source of oxygen on Earth, and thus spread along the surface of the planet. They are present in almost every water source on the surface of the planet and is responsible for the carbon fixation<sup>26</sup>. Their symmetrical structures have attracted interest of researchers; this symmetry allows a more versatile doping of the elements and it widens the possibilities for applications. In hand with the characteristic porosity of diatoms, the surface area increases enormously and thus the effects after doping this element, allowing for a better sensing and monitoring of the material<sup>27</sup>.

Diatoms have shown interesting properties due to its porosity, ease of collection and synthetic reproduction. However, concerning synthetic porous Si, we may find that its development is costly, not as effective as the biological Si structures and even not an easy job for large scale reproduction<sup>28</sup>. Thus, natural Si structures such as diatoms are a great option to do research with since it can be harvested and do not need fabrication<sup>29</sup>. Besides, in combination with plasmonic nanoparticles, it may enhance the luminescence properties and make it more selective, serving as biosensors when a certain compound gets attached to it<sup>30</sup>.

Structurally, diatoms are hierarchically disposed and is widely known for its symmetry. The disposition between pores makes diatoms structures to have an enormous variety of species and thus different properties<sup>31</sup>. The outer structured denominated frustule, is the one made of Silica, composed by two valves valves and held together by girdle bands<sup>29</sup>.

In consequence, the combination of these properties, make diatoms a potential focus of research in the field of biosensors. Some works have already been done concerning doping of the natural element and using its photonic properties for detection purposes<sup>28,32-35</sup>. The photoluminescent properties is well known that could not be assigned to the band gap generated by the amorphous silica structure present in Diatoms. Instead, it is assigned to a variety



Figure 2.2: Optical image of various shapes and different morphology of Diatoms present in water sources. Highly symmetric structures. (Credits and Copyright to <http://golubcollection.berkeley.edu/diatoms/modern.html>)

of surface and point defects, being the strongest contribution, the organic residues incorporated in the silica matrix of the frustule<sup>36</sup>. It has been shown as well, that functionalization might increase enormously different properties of dielectric materials such as morphological or photoluminescence, specially for sensing, optoelectronics or biomedicine<sup>37</sup>.

Functionalization, thus, is an important topic to arrive and different ways of approaching it. Some examples of this are shown in A. Rogato<sup>1</sup>, where different functionalization methods are analysed depending on the purpose and the available materials; these include: Metabolic Doping, Metabolization for Application in Plasmonic, for Protein Immobilization, among others. The last one is of our interest, since we use chemical methods for doping the frustule of Diatoms with the purpose of increasing the photoluminescent properties and change it after a protein or specific agent gets attached to the material.

## 2.0.7 Plasmonic nanoparticles

Noble metal nanoparticles have the capacity of forming localized surface plasmon resonances (LSPR) and thus increase enormously the local electromagnetic field. For this purpose, Gold and silver nanoparticles are the most used since both of them absorb and scatter light in the visible range<sup>38</sup>. In the case of diatoms, it has already been shown that Surface Enhanced Raman Spectroscopy (SERS) displays a huge increment on its signal by the addition of either Ag or Au nanoparticles<sup>39,40</sup>.

### Silver nanoparticles

Silver nanoparticles (Ag NPs) have been studied for a long period until now, having a great number of applications, due to his chemical stability, catalytic activity, surface plasma resonance<sup>41</sup> and even biocompatibility, since toxicity and the before mentioned properties, depend on the size, shape or type of metal they are attached to<sup>42</sup>. An example of this, is shown in Fig. 2.3, where hexagonal, pentagonal, triangular or circular shapes can be observed. This is due to the high sensitivity of the created salt and reducing agent, to environmental or external conditions such as temperature, concentration, pH or reducing agents<sup>43</sup>.

Luminescence in Ag NPs is mainly attributed to the exchange of electrons from the "sp" band to the holes at the "d" band, increased by the surface plasmon resonance<sup>45</sup>. These ones have as well an absorption peak at around 420, which can be tuned depending on the particle size and shape<sup>46</sup>. Two main peaks of emission have been observed, being one in the UV region and the other at around 500 nm or above, depending on shape, size and additional components<sup>47</sup>.

Low skin penetration compared to gold, showing a very low one for intact skin and much stronger in damaged skin. It prevents wound inflammation and hence promoting wound healing in the form of topical administration<sup>41</sup>. In matter of toxicity, Samberg performed a study in vivo skin and in vitro with keratinocytes for washed, unwashed and carbon coated Ag NPs, where he and his team found that it is safe to use coated and washed silver nanoparticles, while toxicity increases for unwashed nanoparticles due to residuals<sup>48</sup>. However, administration via inhalation or subcutaneous injection showed more toxicity, compared to other nanoparticles, tested in organs like brain, liver, kidney and lungs<sup>49</sup>.

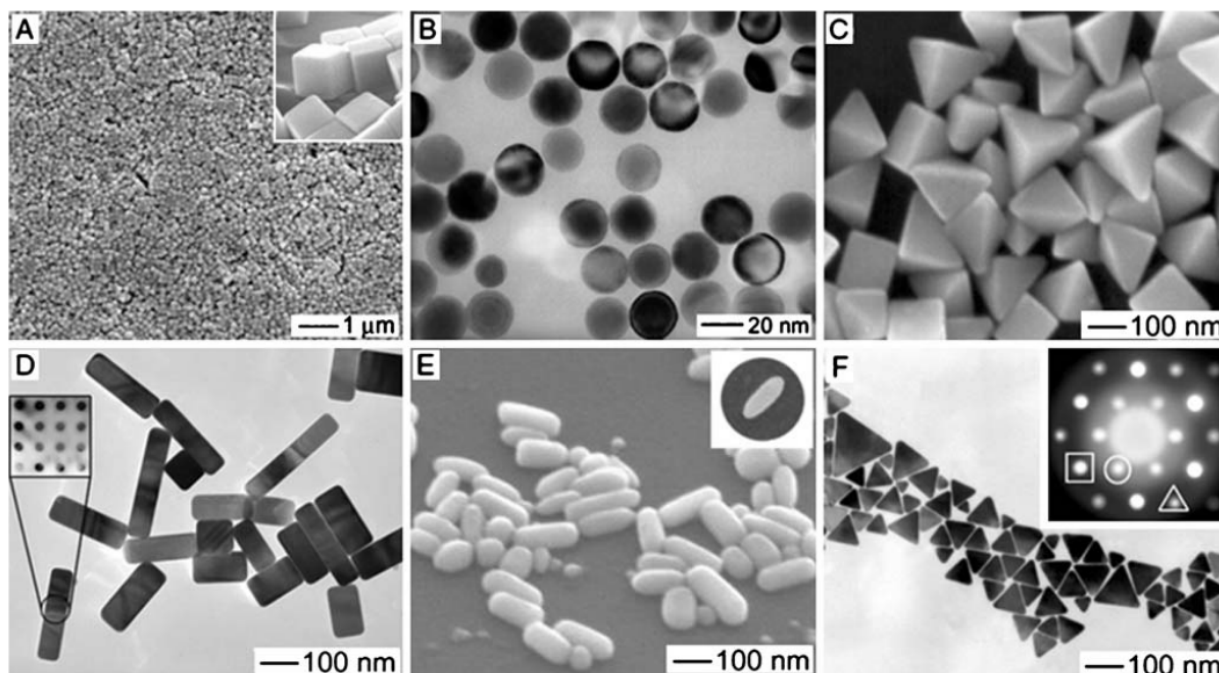


Figure 2.3: TEM/SEM images of Silver Nanoparticles with different shapes, starting from SEM of nanocubes (A), TEM of nanospheres (B), SEM of bipyramids (C), TEM of nanobars (D), SEM of nanorice at  $45^\circ$  (E) and TEM of nanoplates (F). Adapted from<sup>44</sup>.

### Gold nanoparticles

Gold Nanoparticles (Au NPs) show a different colour compared to gold particles, thus a red or dark yellowish colour, with an absorption wavelength of around 520 nm for nanospheres and particle size of 10 nm<sup>50</sup>. This type of nanoparticles has shown low antibacterial properties, as well as variability of methods for the synthesis<sup>51</sup>. Various shapes and sizes, shown in Fig. 2.4 also may serve for different purposes, being the spherical and rod-shapes the most used ones for biomedical applications<sup>52,53</sup>.

As mentioned before, Au nanoparticles, along with Ag NPs, are widely used and they both share the property of having Surface Plasmon Resonance (SPR), which is useful for bioimaging or sensing purposes<sup>54</sup>. Besides that, gold NPs are good for working with light to heat conversion and hence is suitable for photothermal treatments<sup>55</sup>. In the

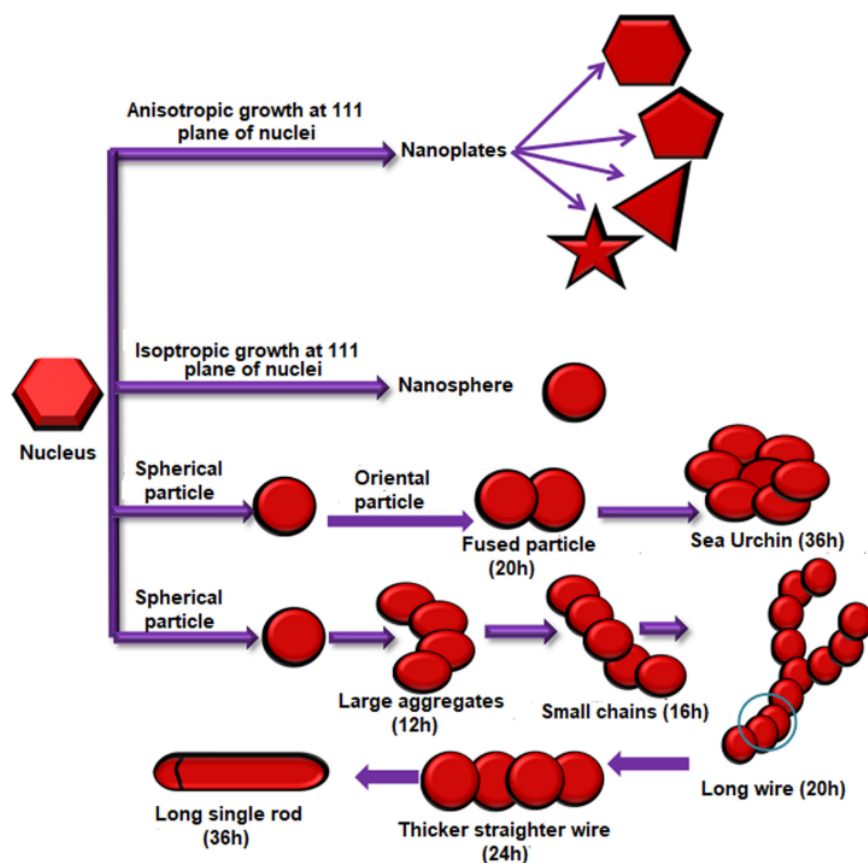


Figure 2.4: Variety of shapes and thus properties of gold nanoparticles. Different synthesis methods are required for each of them. Adapted from<sup>51</sup>

case of Au, an emission peak appear at around 440 nm and correspond to the energy gap between the upper d-band or sp-band to the Fermi level energy<sup>47</sup>.

Furthermore, concerning toxicity, with cultured cells, it has been shown that Au NPs have a low toxicity<sup>56</sup> and it might be reduced with the combination of scaffolds like collagen<sup>57</sup>. Even more on their biocompatibility, they are capable of reducing the production of reactive oxygen and nitrite species and thus contributing to inflammatory process useful for healing<sup>58</sup>.

## 2.0.8 Diatoms doped with Luminescent Elements

Consequently, using diatoms as template for luminescent nanoparticles reduction seems to be an interesting approach. Besides, by now some studies have already tackled this problem and proved meaningful improvements after the doping process with a variety of methods<sup>59,60</sup>. In particular, for the purposes of this study, the focus is on doping frustules with plasmonic-metallic nanoparticles such as Au or Ag. Thus, in the following section some examples and recent approaches within this matter are shown.

### Diatoms with Plasmonic Nanoparticles

Using frustules as a template has shown to be a promising element for applications into the Plasmonics field. One of the main techniques used to test this property is the Surface Enhanced Raman Spectroscopy (SERS), due to the localised surface plasmon contribution and since the signal enhancement factor can directly be calculated, namely:

$$EF = \frac{I_{SERS} / N_{surf}}{\frac{I_{RS}}{N_{vol}}} \quad (2.1)$$

where  $I$  stands for the intensity on each of the techniques and  $N$  represents the number of molecules present on the SERS scattering area or molecules present at the bulk scattering volume<sup>1</sup>. A variety of studies have shown clear examples of efficient intensity enhancement with SERS<sup>61-63</sup>.

## 2.0.9 State of the Art

The use of diatoms as a SERS substrate is widely spread by now, and different approaches have been proposed. Rogato et al.<sup>1</sup> state the thermal deposition method as the most straightforward and simple way to obtain a diatom-based SERS substrate, as well as point out the importance of the morphology and geometry depending on the specific application. Silver and gold NPs have been widely used as metallic plasmonic nanoparticles during the last years and their applications for sensing purposes has conducted enormous research. Comparable particle size to the incident wavelength produces opens up the possibility to work with the Localized Surface Plasmon Resonance (LSPR) and use it in terms of enhancing signal. Thus, this effect is very sensitive to changes in morphology, size and geometry of the material<sup>64</sup>. Representing both an advantage, due to the tunability of the composite, and a disadvantage, since the used methods have to be specific to the geometry and depends on the application, causing problems for easy

replicability at larger scales in most of the cases.

Specifically about diatom substrate Au-NPs, it has already been used for sensitive analysis, enabling molecule sensing for a variety of applications<sup>30</sup>. The latter uses photo-deposition method for Au growth, where timely injections were applied to suspended diatoms for 1h period. Further methods have also been applied, such as the sputtering technique with nanoimprint diatoms, proposed by Cai (2020), showing an enhancement factor of  $10^7$ <sup>65</sup>.

In the case of silver nanoparticles, in-situ methods have already been proposed, as the one proposed by Chang (2010)<sup>66</sup> and further used recently by Konog (201)<sup>67</sup>. This last study proposed the attachment of both Gold and Silver Nanoparticles on top of diatoms, first decorating diatoms with Au NPs by self-assembling methods and then Ag NPs by in-situ growth. While Ren tested the self-assembling method as well for Ag NPs<sup>4</sup>, reaching an enhancement factor of times compared to Ag NPs on glass. Finally, the latest approach has been the formation of nanodendrites (Diatoms-Ag) with highly fluorescent properties<sup>68</sup>.

## 2.1 Characterization Techniques

### 2.1.1 Raman Spectroscopy

Raman Spectroscopy is one of the techniques that takes advantage of the vibrational modes within the molecules in order to determine its molecular structure<sup>69</sup>. Specific vibrations occurring along the sample allow the determination of a specific transition and thus a specific molecule. This technique is based on the Raman effect, which consists of an inelastic scattering of the incoming light<sup>70</sup>.

The usual elastic scatter of light is denominated Rayleigh Scattering, where electron transitions take place and the frequency of the incident photon is the same as the emitted photon. However, in the case that these frequencies are different, Raman effect takes place and can thus produce either Stokes or Anti-Stokes spectra<sup>72</sup>. The difference between these two relies on the emitted frequency, where, in case that the emitted frequency is lower than the incident frequency, it is called Stokes lines. While in the other case, higher frequencies of emitted light with respect to the incident one, are denominated Anti-Stokes lines.

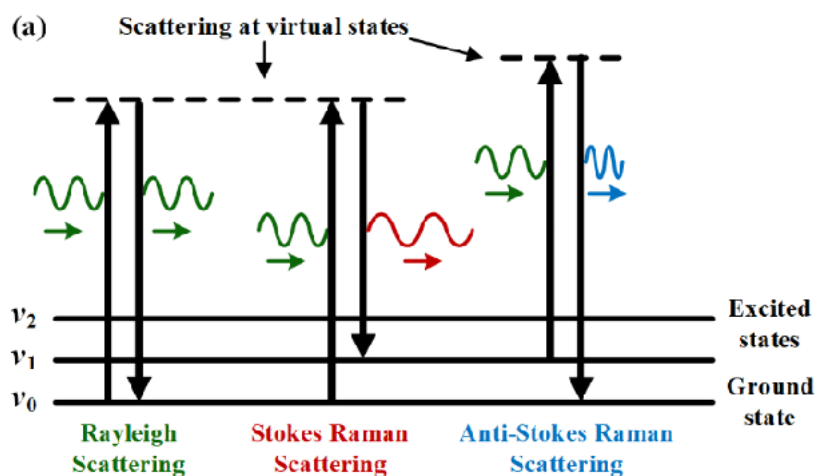


Figure 2.5: Vibrational spectroscopy principles where the three main transitions are shown, namely Rayleigh, Raman Stokes and Anti-Stokes, have higher to lower intensity in this order. These last two correspond to lower emitted photon frequency and higher emitted photon frequency respectively. Modified from Chen (2019)<sup>71</sup>.

Raman Spectroscopy, thus, is used for atomic composition detection, since the shift in energy caused is specifically for the atomic constitution and molecule vibrations<sup>73</sup>. Use of different light sources might cause an enhanced signal in the raman spectrum. For example, the use of an Infrared light source, could decrease the fluorescence background on the signal<sup>73</sup>. This permits to expand the range of applications even for corrosion detection in samples.

Thus, the working principle of this technique is focused on detecting inelastic scattered light of different frequencies than the monochromatic source. For this purpose, a monochromatic light source is needed, which as shown in Fig. 2.6, used a mirror to properly point the laser through a microscope objective and then towards the sample. After reaching the sample, photons emitted by the sample cross the objective and reaches a beam splitter, which reflects only photons coming from the sample. These photons, however, need to be filtered and let only pass the ones at a certain frequency range, thus raman scattering. For this, a focusing lens is used, followed by a notch filter and finally reaching the spectrometer where light is splitted and is detected by the CCD detector.

Furthermore, a specific and widely used technique derived from Raman Spectroscopy, is Surface Enhanced Raman Spectroscopy (SERS). This refers to the adsorption of the sample onto a sample metallic surface, which

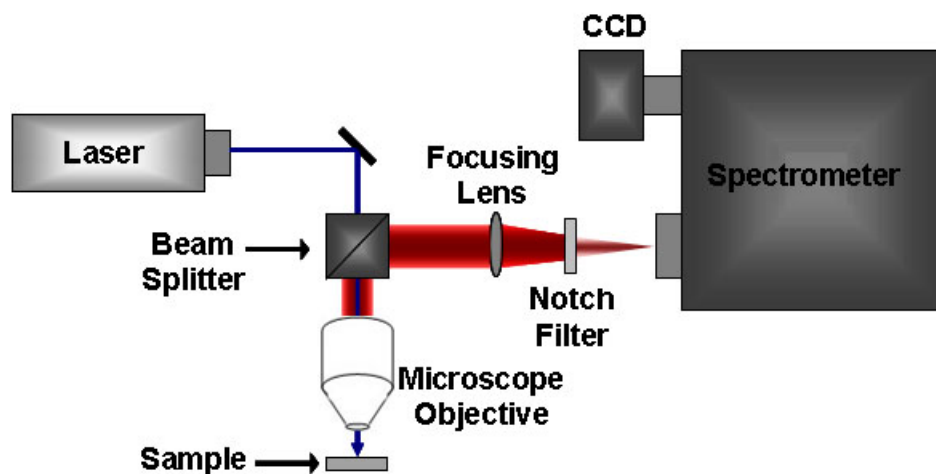


Figure 2.6: Raman Spectroscopy working principle and components. Adapted from Raja<sup>74</sup>.

quenches the effect of fluorescence and enhances raman signal intensities<sup>75</sup>. However, the same effect can also be achieved in a different form and thus considered SERS effect. Here, to enhance raman signal, metallic nanoparticles are adsorbed onto the surface of the sample and thus locally enhancing raman signal and the quenching effect<sup>76</sup>. This enhancement can either be reached by a metallic substrate or considering the probe enhanced with metallic nanoparticles, all of these with certain considerations further analysed by Eric C. et al (2009)<sup>77</sup>.

SERS enhancement has been previously explained by two main theories: electromagnetic (EM) and chemical enhancement, both by placing metallic compounds near the sample molecules<sup>78</sup>. In the case of EM enhancement, it occurs when incoming light is in resonance with metallic nanostructure modes and thus creates a localized surface plasmon resonance. This effect, later on induces localized dipoles, which in consequence increases the electric field around the metallic structure. Finally, the enhanced electric field interacts with the sample, creating an induced dipole and enhancing raman signal by interaction with the incoming EM radiation<sup>78</sup>. In contrast, chemical enhancement comes by direct contact between sample and metallic structures, where new electronic states are formed and thus possible resonating energies.

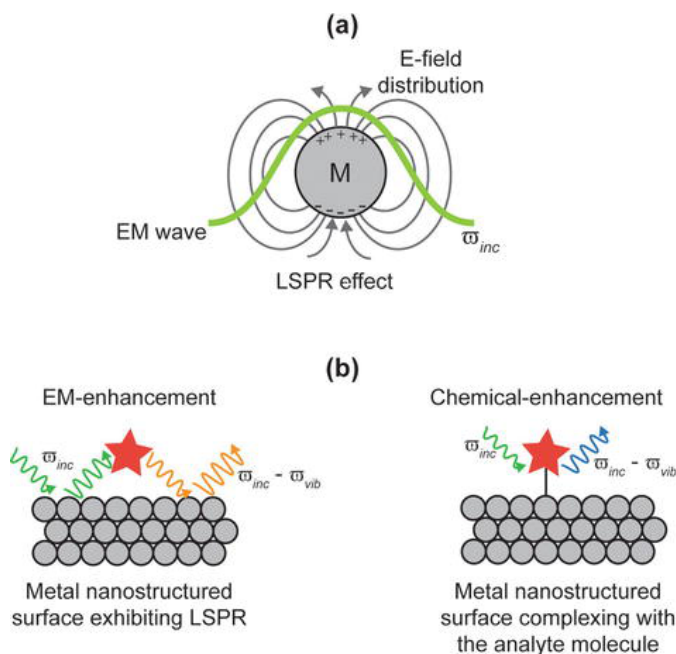


Figure 2.7: Localized surface plasmon resonance (LSPR) by a metallic nanoparticle after exposure to an electromagnetic field, which is the basic concept for SERS or enhanced Raman signal. Both EM and chemical enhancement are shown here. Adapted from Bora<sup>78</sup>.

### 2.1.2 Ultraviolet-visible Spectroscopy (UV-Vis)

UV-Vis Spectroscopy principles rely on light absorption at a certain wavelength, depending on the material, as shown in Fig. 2.8. This is due to molecular excitation, where the transmitted light through the material is governed by Beer-Lambert Law. This law, as mentioned by Chen et al. (2013)<sup>79</sup> is dependent on the incoming light intensity ( $I_o$ ), transmitted light intensity ( $I$ ), or also by the molar absorptivity coefficient of the material ( $\epsilon$ ), concentration of the absorbing species ( $c$ ) and path length of the light through the sample, as shown in the following equation:

$$A = \epsilon cl = \log_{10}\left(\frac{I_o}{I}\right) \quad (2.2)$$

This technique does not require a complex setting up but depending on the quality of its components, more accurate spectra can be obtained. In first place, a light source is needed which is a white lamp. Light coming from the lamp will reach a monochromator which allows to separate different wavelengths, to further measure one

wavelength at a time. Filtering each wavelength is made by a slit with a certain spacing and is the previous component before reaching the sample. Finally, the light at a certain wavelength will reach and cross the sample until it arrives at the detector. Specific wavelengths will be absorbed by the sample and thus they will not arrive at the detector, shown at the final absorption spectra.

It is used widely for assessing the presence or absence of a certain molecule or composite into the sample. The technique itself is highly reproducible and thus is a key component for first characterization steps. Even more, the technique allows to assign the band gap when working with semi-conducting elements. However, this matter must be tackled carefully since wrong assignments often occur, leading to wrong conclusions. The cause of the latter, is due to the dependence on the observer to assign the slope of the tangent in UV-Vis absorption, but also due to the variety of effects that occur at the same time in the sample. These effects concern the path of light such as transmittance, reflectance, scatter light, specularly reflected light or diffusely reflected<sup>79</sup> and even changes in absorbance due to the substrate or morphology of the sample.

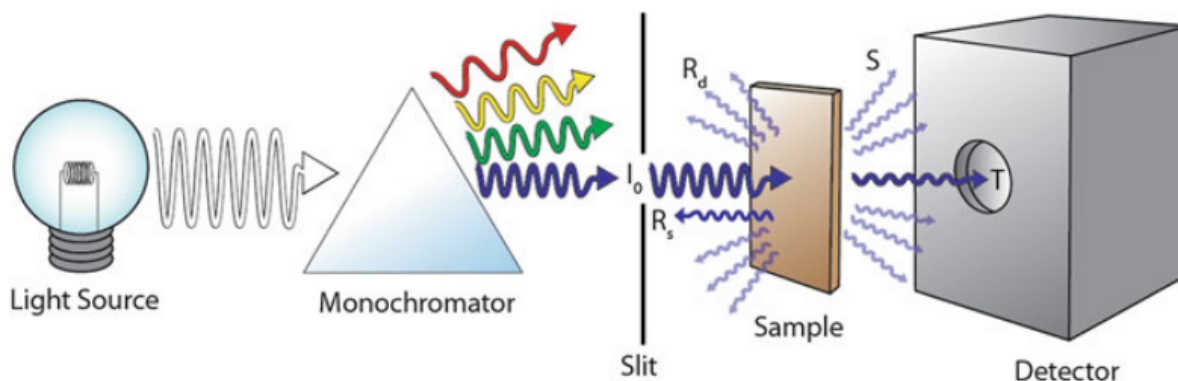


Figure 2.8: UV-Vis working principle from the light until reaching the sample and capturing the outgoing signal. Adapted from<sup>79</sup>.

### 2.1.3 Scanning Electron Microscopy (SEM)

Electron Microscopy could be considered as a step forward light microscopy in matters of resolution, since it captures the released electrons from the material to generate a high quality image, reaching even the nano-meter scale for high quality Scanning Electron Microscopy (SEM). The working principle concerns the irradiation of the sample by the use of an electron beam within 1 to 30 kV energy range<sup>80</sup>. This, causes the release of both photons and secondary electrons from the sample surface or inside the material which reach the detector and the image is generated computationally. Mainly serving for specimen shape analysis for structures with sub-micron structures<sup>81</sup>, as shown in Fig. 2.9.

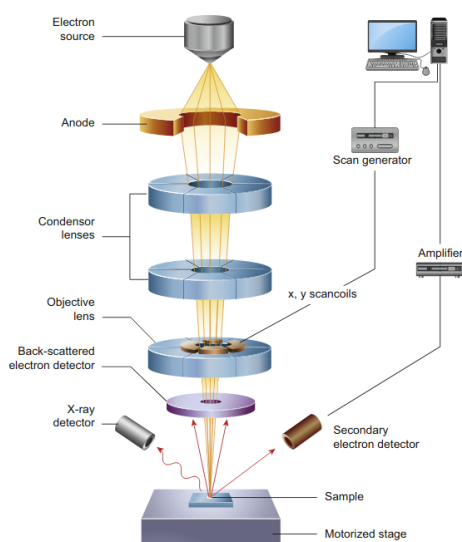


Figure 2.9: Scheme of SEM imaging, where the usual components are shown. Here, the secondary electrons, scattered from the sample, are used to generate the image. Adapted from Inkson (2016)<sup>81</sup>

In contrast, these advantages in resolution come by the hand of certain compromises, since the use of electrons in microscopy requires the sample to be in vacuum and use of high electron energy<sup>81</sup>. Thus, requiring the sample to stand high energies, with the risk of damaging the sample. An example, is the imaging of biological samples or ones that have soft compositions, which has opened up a wide field of study. In consequence, sample preparation has become an important requirement before using electron microscopy, as well as.

Most SEM analysis are carried out on dry samples, thus wet samples are the most challenging to prepare and

analyse<sup>82</sup>. In general terms, it is important to consider that our samples have to be dried before SEM acquisition in case the equipment is not set for this purpose. Furthermore, the energy of the excitation beam has to be carefully adjusted, taking into account that high energies might give us better quality but the risk of damaging the sample increases. Biological samples in general are hard to treat since they are poorly conductive. More detailed steps, depending on the samples the researcher is working with, are further explained by Echlin & Patrick (2009)<sup>82</sup>.

#### 2.1.4 Scanning Transmission Electron Microscopy (STEM) mode in SEM

Similar to the before mentioned, SEM microscopy, Scanning Transmission Electron Microscopy (STEM) also uses electrons as source for the imaging process. However, STEM mode in SEM requires an additional component to the full SEM set up, which is a STEM detector right below the sample to capture transmitted electrons. An scheme of this technique is shown in 2.10. The main difference between TEM and STEM is the scanning option, where the beam is highly focused at a specific point and further improved to scan a certain area, as well as the aberration-correction implemented in STEM<sup>83</sup>. Due to the focused electron probe, allow the detection of different scattered electrons in function of the position of the beam<sup>84</sup>.

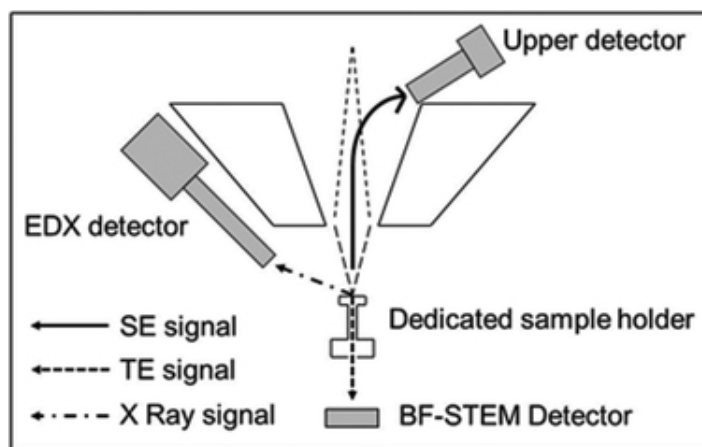


Figure 2.10: Light path and set up of STEM mode in SEM. The transmitted electrons are captured by the STEM detector placed below the sample holder<sup>85</sup>

One of the features used in this study, is the dark field mode, which consist of a wide angle detector that captures only elastically scattered electrons by constituent atoms of the macro-molecule<sup>86</sup>. This, allows identification of

plasmonic nanoparticles from other particles that also create a contrast in the usual STEM imaging feature.

Even if the scanning feature is useful and allows a better visualisation for high quality STEM equipment, it is also very sensitive to external parameters. Thus, temperature, vibrations, electromagnetic or acoustical waves and air pressure have to be controlled and reduced in the room<sup>87</sup>.

### 2.1.5 Photo-luminescence Excitation (PLE)

Photo-luminescence Excitation (PLE) technique refers to the detection of the emission spectra of a certain sample after exciting it with light at a range of wavelengths. PLE shares the same working principle as the PL technique. However, the difference relies on the detection of the emitted light, since PLE detects emission at a specific wavelength with a defined wavelength excitation; while PL detects the full range of emission at a defined wavelength excitation<sup>22</sup>. A scheme of the process is shown in Fig. 2.11.

An scheme of the electron-pair generation is shown in Fig. 2.1, where an incoming ray of light excites the material until it reaches the sample, visualised in the working principles of fluorescence microscopy in Fig. 2.11. The lamp or any other light source, strong enough, provides energy and makes an electron at the Valence band to jump towards the Conduction band, creating an electron-hole pair. The dichroic mirror allows to guide the specific wavelength towards the sample and at the same time serves as an initial filter for a certain range of wavelengths, while the emission filter allows to pass only the light emitted by the sample.

These transition energies occurring internally open up a variety of possibilities depending on the type of transitions occurring into the sample. For instance, inelastic transitions, where the electron does not come back to the initial position and generates Raman signals. In matters of luminescence, there is an important process when talking about sensors or bioimaging material, which is fluorescence. In the coming section more about this will be discussed.

### Fluorescence Microscopy

The key advantage of this technique is due to the contrast of the image, where the fluorescent materials (fluorochromes) can be detected even at lower resolutions of the microscope. This is due to the high energy excitation, that causes the release of photons at the visible range. Besides, it is further used in samples with lower concentrations or even for generating 3D images, depending on the mode it is being used<sup>88</sup>. Fluorescence microscopy is widely

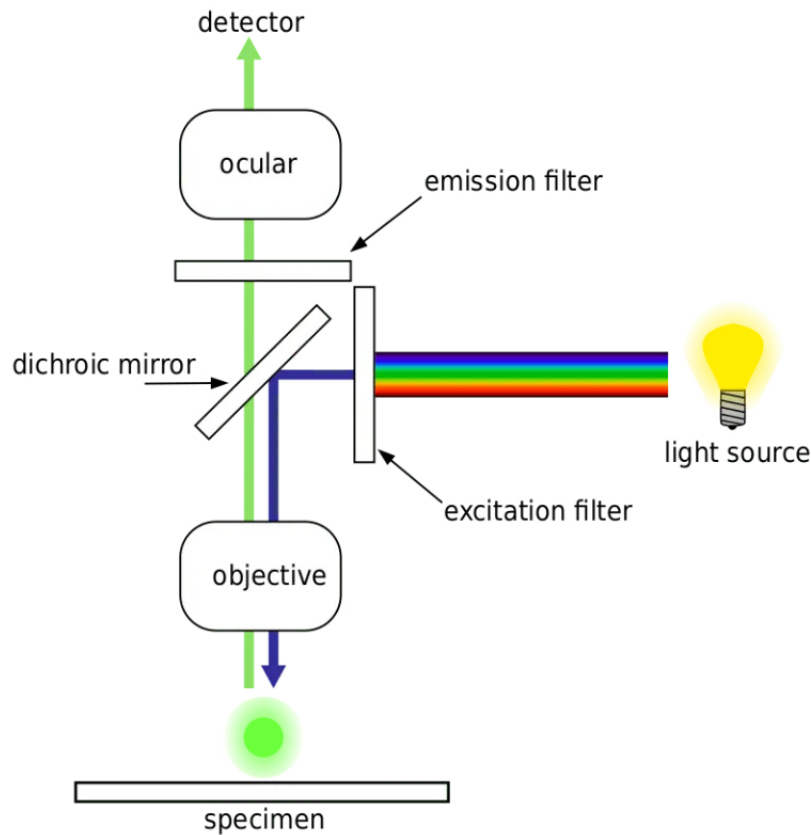


Figure 2.11: Fluorescence microscopy working principle, showing the path that light goes through, until photons from the sample reach the detector. Photo credit: Henry Mühlpfordt.

used for biological and medical applications. It is commonly seen for living cells or tissue due to the small particle detection.

More specifically, the working principle used in this study, used a lamp that illuminates from below the sample and the microscope lens is placed above the sample. Thus, fluorescence light emission is measured with a range of emitted wavelength, instead of a laser excitation. Later on, the acquired images can be taken at various augmenting lenses; for our purposes, obtained images were further processed to obtain an approximate emission wavelength.

## 2.1.6 Fourier Transform Infrared

Fourier Transform Infrared spectroscopy (FTIR) is generally used for identification purposes, since each molecule has its own fingerprint in FTIR spectra. The obtained signal from this technique is in the range of 400 to 4000  $cm^{-1}$ , in which any perturbation from the obtained absorbance pattern, would represent a certain bonding or compound<sup>89</sup>. Both an excitation laser and an Infrared light is needed to obtain a FTIR spectra. Interference of these light sources goes through the sample and reach the detector to further be processed and performed the Fourier transform to obtain a readable spectra. An scheme of this working principle is shown in Fig. 2.12.

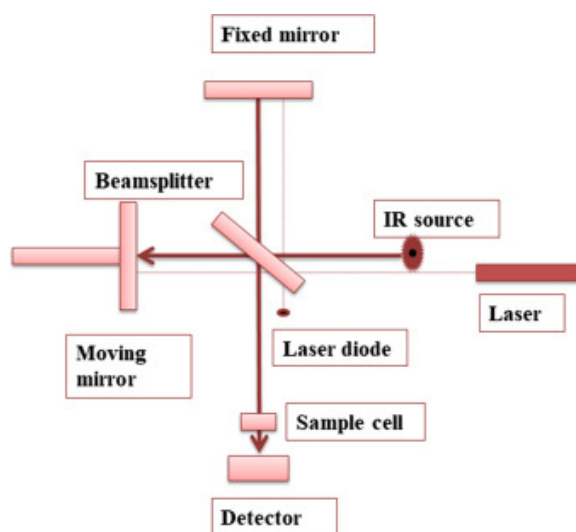


Figure 2.12: Fourier Transform Infrared working principle and light path until it reaches the detector. Adapted from Titus<sup>89</sup>.

A table with the most common bonds and molecules is shown in 2.1. All these perturbations are well identified in literature and due to this replicability, it is commonly used for daily-life problems such as illegal substance identification. Furthermore, the variety of applications allow to follow processes such as UV modification in samples, surface grafting, plasma treatment, among others that are further described by Mohamed et al. (2017)<sup>90</sup>.

Type of Bonds	Wavenumber Value (1/cm )	Intensity
C-H	3000-2850 (alkanes stretch)	s

Type of Bonds	Wavenumber Value (1/cm )	Intensity
	1450 and 1375 (alkanes: -CH <sub>3</sub> bend)	m
	1465 (alkanes -CH <sub>2</sub> e bend)	m
	3100-3000 (alkenes stretch)	m
	1000-650 (alkenes out-of-plane bend)	s
	3150-3050 (aromatic stretch)	s
	900-690 (aromatic out-of-plane bend)	s
	3300 (alkyne stretch)	w
	2900-2800 (aldehyde)	w
C=C	1680-1600 (alkene)	m-w
	1600 and 1475 (aromatic)	m-w
CO	2250-2100 (alkyne)	m-w
C=O	1740-1720 (aldehyde)	s
	1725-1705 (ketone)	s
	1725-1700 (carboxylic acid)	s
	1750-1730 (ester)	s
	1680-1630 (amide)	s
	1810 and 1760 (anhydride)	s
	1800 (acid chloride)	s
C-O	1300-1000 (alcohol, ethers, esters, carboxylic acids, anhydrides)	s
O-H	3650-3600 (free alcohols, phenols)	m
	3400-3200 (H-bonded alcohols, phenols)	m
	3400-2400 (carboxylic acid)	m
N-H	3500-3100 (primary, secondary amines and amides: stretch)	m
	1640-1550 (primary, secondary amines and amides: bend)	m-s
C-N	1350-1000 (amines)	m-s
C=N	1690-1640 (imines and oximes)	w-s

Type of Bonds	Wavenumber Value (1/cm )	Intensity
CN	2260-2240 (nitriles)	m
X=C=Y	2270-1940 (allenes, ketenes, isocyanates, isothiocyanates)	m-s
N=O	1550 and 1350 (nitro: R - NO <sub>2</sub> )	s
S-H	2550 (mercaptans)	w
S=xO	1050 (sulfoxides)	s
	1375-1300, 1350-1140 (sulfones, sulfonyl chlorides, sulfates, sulfoamides)	s
C-X	1400-1000 (fluoride)	s
	785-540 (chloride)	s
	<667 (bromide, iodide)	s

Table 2.1: FTIR wavenumber list with the corresponding types of bonds that could be assigned to a certain range. Here, s, small; m, medium; w, wide. Adapted from<sup>90</sup>



## Chapter 3

# Methodology

### 3.1 Chemicals

Diatoms were collected by PhD German Martín Merino and received by PhD Gema González with permission of use for research purposes. These were collected at the Guayllabamba intermountain basin, Ecuador, being of species *planktonic* and genus *Aulacoseira* in form of rocks. Hydrogen peroxide ( $H_2O_2$ ), Sulfuric acid ( $H_2SO_4$ ) and Trisodium Citrate ( $Na_3C_6H_5O_7$ ) were purchased from Lobachemie . Silver Nitrate ( $AgNO_3$ ), Chloroauric acid ( $HAuCl_4$ ) and Sodium borohydride ( $NaBH_4$ ) were obtained from Sigma-Aldrich. The chemicals were not further modified but they were used as received. Distilled water was filtered and processed at the laboratory, while Ethanol and Isopropil were purchased at M&M representations.

### 3.2 Light Chambers

The light source is tested for the reduction process, hence two different light sources were used (463 and 511 nm). These were disposed in closed chambers following the designed of Saade (2014)<sup>91</sup> with further modifications to provide higher power of light to the chambers, as well as for having light pointing at two different heights of the sample. A scheme of the chambers is shown in Fig. 3.1B along with the experimental setup 3.1C. Since the use of light source is tested for the both Ag NPs and Au NPs, the final number of chambers is four.

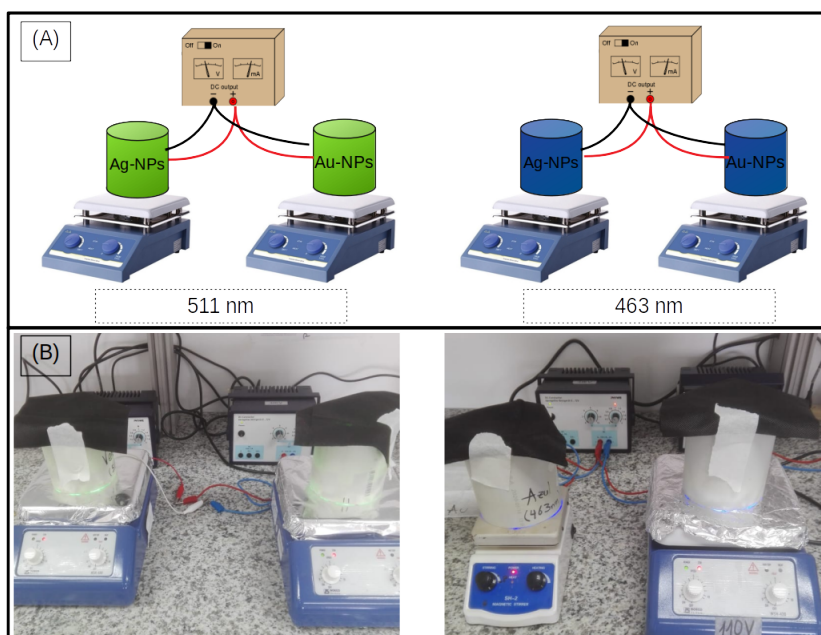


Figure 3.1: Light chambers disposition for two different wavelength and for Ag and Au NPs and constant stirring. In A a scheme of the setup is shown, while in B the real experimental setup is observed

Thick PVC and high power LEDs were used to design the chambers, purchased at a local store. PVC tubes had dimensions of 12 cm in height and 11 cm of diameter, with 2 mm of thickness. LEDs were of 1W power each, where eight of them were placed inside the chambers in a certain disposition shown in Fig. 3.1A, which is a group of two LEDs joined in series repeated 4 times in parallel and a current of 0.7 A for both 463 and 511 nm wavelengths.

### 3.3 Synthesis

#### 3.3.1 Diatoms extraction

Diatoms were recolected from a sedimentary rock, obtaining Diatoms of the species *Planktonic* and genus *Aulacoseira*. These were collected at the Guayabamba intermountain basin, at the San Miguel formation, where diatoms were present as thin layers of white colour inside the rock. For its extraction, it was needed to separate the white varves (internal layers) and softly scrape the surface of the latter, obtaining a white powder. These varves can be

observed inside the rock in Fig. 3.2.



Figure 3.2: Sedimentary rock from which diatoms were extracted. White varves correspond to diatom layers.

Since diatoms probably contain a significant amount of carbon residues, a purification method was performed, where it was exposed to a piranha solution. This would also remove small fragments of other elements, as well as open spots at the surface of frustules, hence promoting nucleation. Afterwards, the diatoms were carefully extracted and centrifuged by adding some Ethanol. The centrifugation process was performed at 5000 rpm for 5 min and repeated 5 times each in order to avoid acid residuals. Finally, it was again extracted and leave it to dry outdoor an entire day.

### 3.3.2 Ag/Au Reduction and deposition on Diatoms

The experimental procedure of reduction and deposition was performed in two different forms in order to test the efficiency of each method. Both reduction and deposition were performed at the same time, following the process

of Onesto et al. (2018)<sup>30</sup>. In first place, the reduction of NPs were performed using only the light source. In second place, for a better performance a reducing agent was used in order to support the reaction and check improvements of NPs formation.

### Ag/Au Photodeposition process

Diatoms were cleaned following the process before mentioned, in this case they were left into  $H_2O_2$  for five days and cleaned thoroughly with Ethanol. After cleaning and left to dry, they were dispersed in distilled water, namely 20 mg of Diatoms in 50 mL of Ethanol. Additionally, 360  $\mu$ L of Sodium Citrate is added in order to softly support the reduction process, as well as for neutralising the pH of the solution. Afterwards, and with constant stirring, 30  $\mu$ L of either Chloroauric Acid ( $HAuCl_4$ ) or Silver Nitrate ( $AgNO_3$ ) (0.1%) were added every 5 min, for a total duration of 1 h.

Furthermore, the solutions were kept at constant stirring and exposed to the light source inside the chambers for 4, 8 and 15 hours. The same process is repeated for both wavelengths (463 – 511 nm).

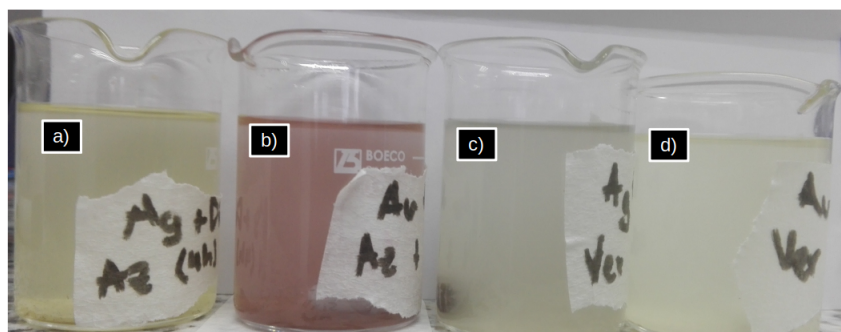


Figure 3.3: Decorated diatoms in solution after 4 hours of exposure to different light sources. These correspond to the photodeposition process group with no additional support. a) Ag NPs-Diatom with blue light, b) Au NPs-Diatom with blue light, c) Ag NPs-Diatom with green light and d) Au NPs-Diatoms with green light.

### Ag/Au Photodeposition-Sodium Borohydride addition

In this case, raw Diatoms were left into the piranha solution made of 80 mL of  $H_2SO_4$  (1M) and 20 mm of  $H_2O_2$  for one hour with 60°C of temperature and cleaned afterwards with distilled water in repeated centrifugation. Properly dried, 50 mg of Diatoms were dispersed in 50 mL of  $H_2O$ . 0.9 mL of both Trisodium Citrate and Sodium Borohydride were added to enhance the reduction process. Finally, same as before, in constant stirring 75  $\mu$ L of either Chloroauric Acid or Silver Nitrate (0.1%) were injected each 5 min for 1h. The ratio diatom vs reactants has been kept the same in order for further comparison.

In contrast to the latter, here the solutions were kept for shorter times (2,4 and 8 hours) inside the chambers with the same light source and intensities.

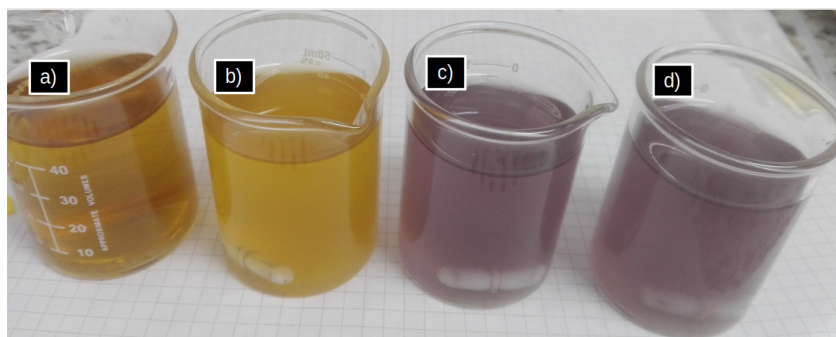


Figure 3.4: Decorated diatoms in solution after 2 hours of exposure to different light sources. These correspond to the Sodium Borohydride addition group. a) Ag NPs-Diatom with blue light, b) Ag NPs-Diatom with green light, c) Au NPs-Diatom with blue light and d) Au NPs-Diatoms with green light.

### 3.3.3 DNA extraction and attachment to diatoms

In first place, to obtain the DNA, bacteria culture was performed of Gram-Negative E. Coli ATCC 25922, which a sample of it was placed in culture medium for 24 hours under 37°C and constant shaking. Afterwards, we used 4 eppendorfs with 1.5 mL of the culture medium each to proceed with the purification DNA kit available at the Biology Laboratory at Yachay Tech University. Thermo Scientific GeneJET Genomic DNA Purification Kit, is the kit used to perform DNA extraction from E. Coli bacterias. Protocol is already defined, from which a summary of the steps is as follows:

- Harvest bacteria cells in a 1.5 mL microcentrifuge tube and centrifugate for 10 min, discarding the supernatant.
- Suspend the pellet in 180  $\mu$ L of their Digestion Solution, followed by 20  $\mu$ L of Proteinase K.
- After shaking thoroughly, the tube was incubated at 56°C in a shaking water bath for 30 min.
- Add 20  $\mu$ L of RNase solution mix and incubate for 10 min.
- Add 200  $\mu$ L of Lysis Solution and vortex for about 15 seconds.
- Add 400  $\mu$ L of 50% ethanol and mix by pipetting or vortexing.
- Transfer lysate to DNA Purification Column from the kit. Centrifuge for 1 min at 6000 $\times$ g. Discard the collection tube with the remaining solution and place the Purification Column into a new 2  $\mu$ L collection tube.
- Add 500  $\mu$ L of the first modified Wash Buffer from the kit. Centrifuge for 3 min at 8000 $\times$ g. Discard the flow-through and place the collection tube into the column.
- Add 500  $\mu$ L of the second modified Wash Buffer from the kit. Centrifuge for 3 min at 12000 $\times$ g.
- Add 100  $\mu$ L of Elution Buffer from the kit to the center of the DNA Purification Column to elute genomic DNA. Incubate for 2 min at room temperature and centrifugate for 1 min at 8000 $\times$ g.
- Repeat the last step with the same quantities and times.
- Discard the purification column. Store purified DNA at -20°C for later use.

## 3.4 Characterization Equipment

### 3.4.1 UV-Vis Spectroscopy

UV-Vis spectra were acquired both in solid and liquid state. In the case of solid samples, diffuse reflectance was used, where similar results were obtained. The model of the machine was LAMBDA 1050+ UV/Vis/NIR, with Accessory Praying Mantis in the range of 190-800 nm at the Yachay Tech University; data interval of 1 nm, scan speed 266.75 nm/min and slit width of 2 nm. For the case of liquid samples, the same conditions were used, with a slit width of 1 nm and double beam.

This spectroscopy technique was used as an initial step along the synthesis process, to verify the presence of both diatom frustules and plasmonic nanoparticles (Ag and Au NPs), due to their specific absorption wavelengths. Upper right corner of Fig. 3.5 shows absorption spectra of Au and Ag nanoparticles, as well as their change with UV light exposure. Moreover, the lower right corner of this figure shows an example of diatoms absorption spectra, thus similar to our expected results.

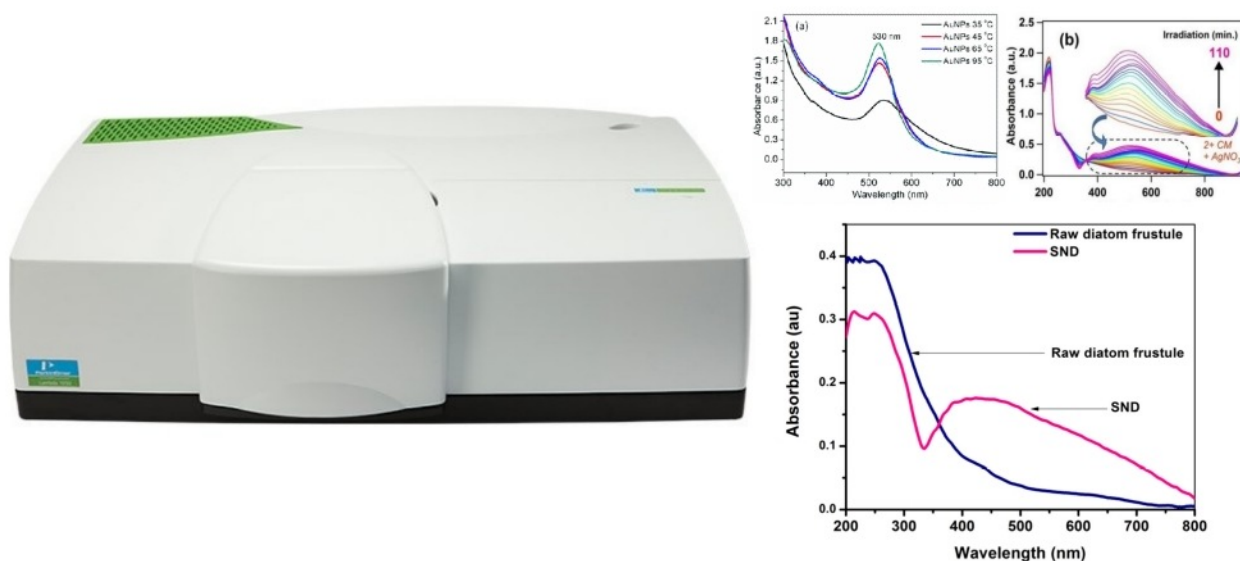


Figure 3.5: LAMBDA 1050 UV-Vis spectroscopy equipment at Yachay Tech University (left). The first spectra (a) shows the absorption peak corresponding to Au NPs, the upper right spectra (b) shows broad peaks of Ag NPs developing with UV light exposure. Finally, absorbance for raw diatom frustule is shown in the lower right corner. Spectra adapted from Kim<sup>92</sup>, Gupta<sup>93</sup> and Chetia<sup>94</sup>, respectively.

### 3.4.2 Raman Spectroscopy

Raman Spectra were acquired with the LabRAM HR Evolution Horiba model, which has two excitation lasers, namely 532 and 633 nm wavelength. This equipment can be observed in Fig. 3.6. For raman measuring purpose, the drop casting method was used, where a silicon wafer was placed over the sample holder. On top of the silicon wafer a drop of the samples was added and let dry for 40 minutes approximately each sample. Measurements were performed with Au coated silicon wafer and non coated silicon wafers, which will be further discussed in the results section.

This technique which is one of the most important techniques to observe the raman signal enhancement after addition of plasmonic nanoparticles, as well as after DNA attachment due to its sensibility to fluorescent light. Fig.3.6 at the upper right side, shows the Raman spectra of Ag nanoparticles, while the lower right corner shows a

comparison of two different excitation lasers on diatoms. This represents some of the expected results on diatoms but also the use of different excitation wavelengths. Within this process, it allows to visualise the SERS effect with metallic nanoparticles but also to visualise the optimal time exposure to light during the NPs in-situ synthesis processes.

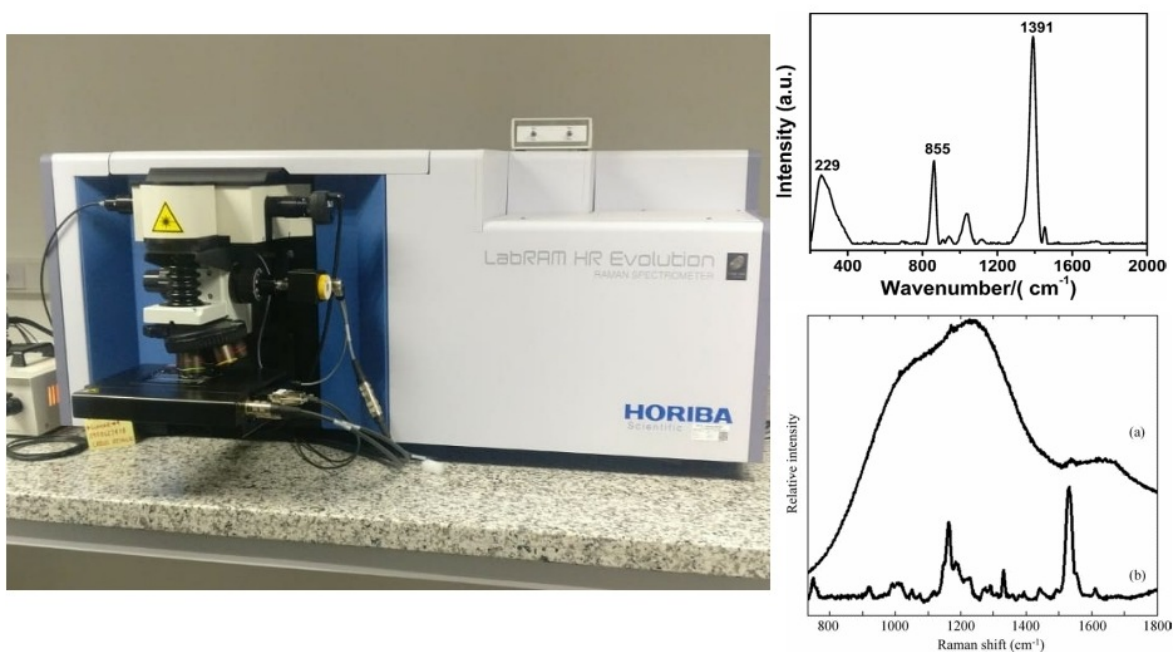


Figure 3.6: LabRAM HR Evolution Horiba model for Raman Spectroscopy analysis (left). Ag NPs raman spectrum at the upper right corner, while diatom frustule spectrum is shown at the bottom right corner. Spectra were adapted from Cai<sup>95</sup> and Meksiarun<sup>96</sup>.

### 3.4.3 Scanning Electron Microscopy (SEM)

Scanning Electron Microscopy micrography was performed with the Phenom Pro X model, with a source of  $CeB_6$  at the Yachay Tech University. Samples were placed over a carbon substrate from solid samples of Diatoms decorated with either Ag-NPs or Au-NPs. An image of the SEM model is shown in Fig. 3.7. In general terms, samples were measured at low vacuum, however, specific details for each samples are described with their respective figures.

SEM microscopy was used to obtain high quality images of diatoms and also to visualize the deposit of Ag and Au NPs on top of diatom frustules. Furthermore, useful information such as average frustule length, pore size and cleaning of the sample was obtained. For this purpose, different imaging conditions were applied and described on each presented image. On Fig.3.7 at the right side, example images of diatoms from the Aulacoseira group, are shown and reflect the expected results.



Figure 3.7: Phenom Pro X equipment used for SEM micrography of diatoms (left) along with SEM images from Aulacoseira diatom groups, similar to the current samples. Bars: Figs. 33-37 =  $2\ \mu\text{m}$ ; Fig. 38 =  $0.5\ \mu\text{m}$ . Micrographies adapted from: [https://www.researchgate.net/figure/38-Aulacoseira-ambigua-external-view-SEM-33-Valve-view-of-the-terminal-cell-of\\_fig4\\_257576830](https://www.researchgate.net/figure/38-Aulacoseira-ambigua-external-view-SEM-33-Valve-view-of-the-terminal-cell-of_fig4_257576830)

### 3.4.4 Scanning Transmission Electron Microscopy (STEM)

Scanning Transmission Electron Microscopy was performed at the Universidad de las Fuerzas Armadas (ESPE), with the TESCAN Mira 3 model STEM mode and Back Scattered Electrons in SEM. Here, size and shapes were determined of plasmonic Nanoparticles. Both SEM and STEM modes were acquired with this equipment, for which SEM imaging samples had the same preparation process as before. However, in the case of STEM mode, a drop of the liquid was placed over a squared holder and let dry at normal conditions overnight. Samples were measured at 30 kV and a working distance of 5.5 mm on average.

This technique was necessary mostly to determine average nanoparticles sizes and shapes, due to the resolution and magnification constraints with SEM imaging. Moreover, the equipment used in a different mode, allowed to obtain a higher contrast SEM image with the In-beam back scattered electrons. Some STEM images from both Ag and Au NPs are shown in Fig. 3.8.

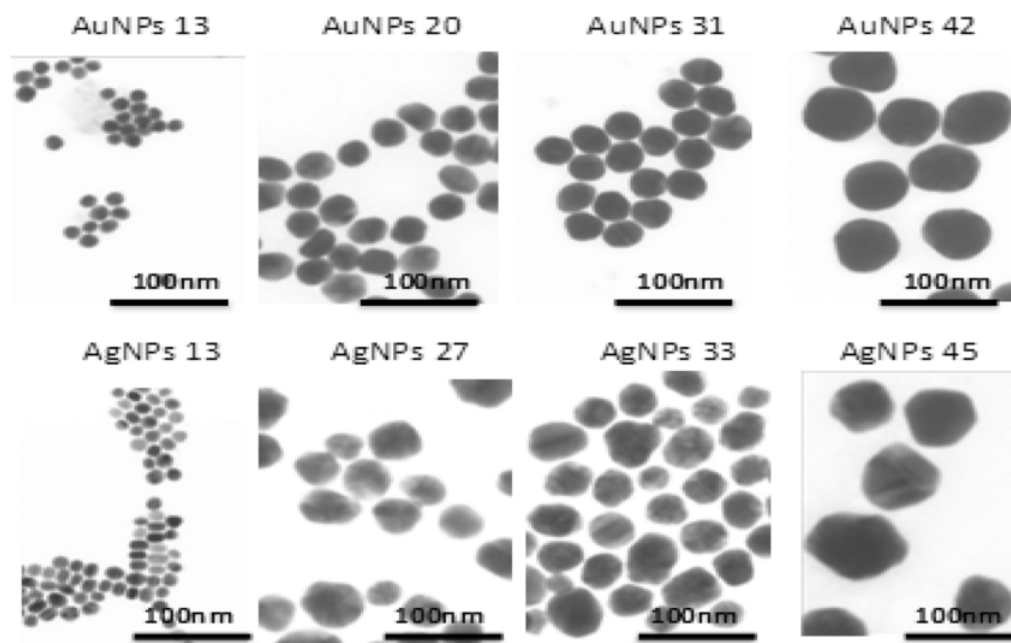


Figure 3.8: STEM images of both Ag and Au nanoparticles, from which sizes and shapes can be obtained after some image processing. Adapted from Pudlarz<sup>97</sup>.

### 3.4.5 Fluorescence Microscopy

Fluorescence imaging was performed with the Olympus BX63 microscope, with the fluorescence module, along with the DAPI complement for blue (433 nm) and green (532 nm) light. Samples were prepared by dripping about 5mL of decorated diatoms on top of the sample holder and let it dry at room temperature. With this imaging technique the different fluorescence emission wavelength was expected to observe, as shown in 3.9. Besides, to notice the difference before and after DNA attachment to doped diatoms and thus, to serve as an additional proof of the use of diatoms as biosensors.

Some of the expected results concerning fluorescence microscopy, have to do with the verification of fluorescence in diatoms themselves and how it might change with plasmonic nanoparticles addition, along with DNA attachment. An example image is shown in Fig.3.9 at the right, where diatoms were embedded into yellow fluorescence beads to enhance fluorescent signal.

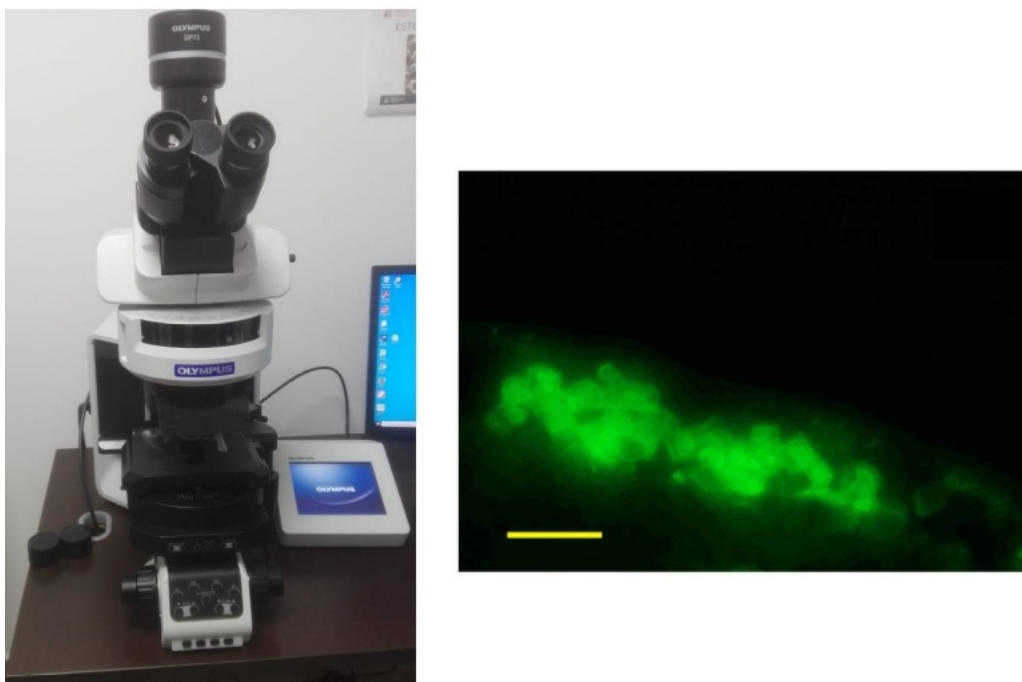


Figure 3.9: Microscope used for fluorescence imaging into the Fluorescence mode of the equipment. The right hand image shows the fluorescence image taken after immersing diatoms in Yellow fluorescent beads for enhancing the fluorescent signal, here the scale bar is 50  $\mu\text{m}$ . Adapted from Villani (2019)<sup>98</sup>.

### 3.4.6 Fourier Transform Infrared spectroscopy

The Fourier Transform Infrared spectrum was taken using the AGILENT Cary-630 FTIR spectrometer, which belongs to Yachay Tech University and is located in the sample preparation laboratory of the School of Chemical Sciences and Engineering, shown in Fig. 3.10. Samples were measured in solid state, thus they were let to dry at normal conditions and used the remaining solid diatom frustules to measure FTIR spectra.

Infrared spectroscopy was intended to show information about the composition and molecular compounds present in the sample, Specifically, it was used to observe the evolution of the samples before DNA attachment and different times of light exposure during NPs synthesis, could affect the molecular compounds concentration. Some of the expected results concern the identification of DNA attachment on diatoms, as shown in Fig. 3.10 at the top right corner, as well as diatoms compounds identification, shown in Fig.3.10 bottom right corner, and their change over

light exposure.

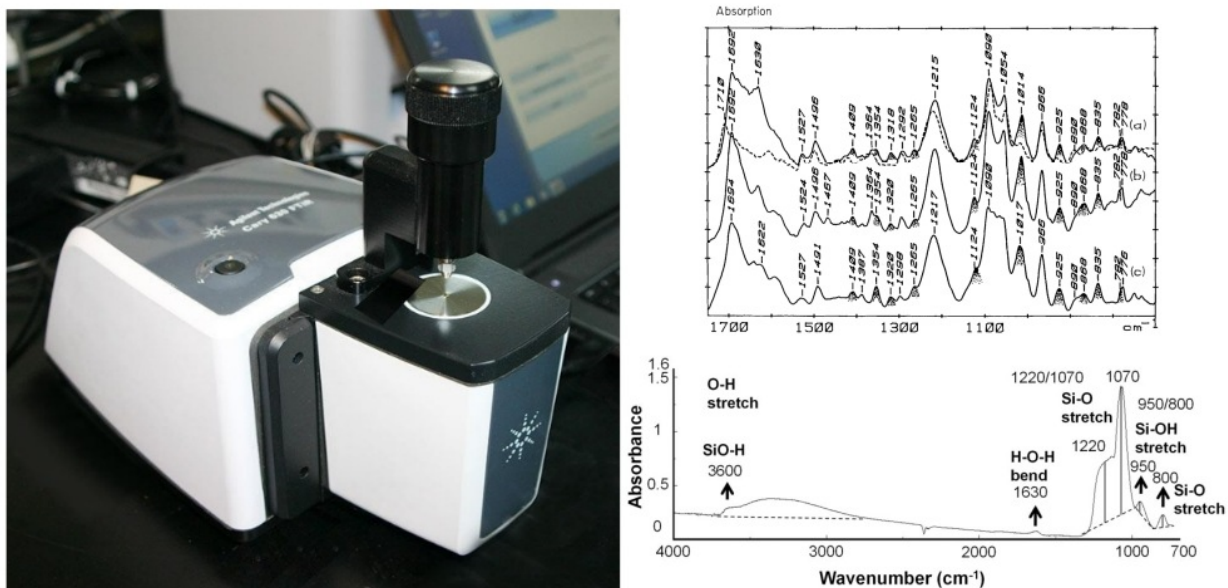


Figure 3.10: AGILENT Cary-630 FTIR spectrometer with the solid sample header (left). DNA FTIR absorption spectrum at the upper right corner, and diatom frustules FTIR spectrum below. Spectra were adapted from Taboury<sup>99</sup> and Alipour<sup>100</sup>, respectively.

## Chapter 4

# Results & Discussion

### 4.1 Diatoms decoration process

Diatoms present a variety of shapes and come from many different sources. In this case, diatom frustules extraction was carried out from a sedimentary rock, from which a cleaning and decoration process needs to follow. These last steps are further explained and analysed in the coming sections.

#### 4.1.1 Diatoms cleaning

Since frustules come from living organisms, the carbon content is significant, increased by deposition along the varves from which the extraction process was performed. Thus, a cleaning process is necessary to work with them afterwards. For this, firstly an acidic solution ( $H_2SO_4$ ) was used to remove carbon content and to slightly damage the surface of frustules for the next step, which consist in the addition of peroxide ( $H_2O_2$ ) to create hydroxyl groups on frustules for better NPs in-situ synthesis. After this piranha treatment, washing with either Ethanol or distilled water was carried out several times to assure acid removal. Final results after frustule cleaning can be observed in microscopy images, where still some carbon contents appear.

#### 4.1.2 Diatoms surface decoration Au/Ag Nanoparticles

Frustules at this point are ready for further processes. Here, the addition of Sodium Citrate serves to support the reduction process and to neutralise the pH of the solution. Light is then used as a reductor agent, which acts by

reducing the salt introduced afterwards. This creates a ionic compound that joins hydroxyl groups available at the surface of diatoms. Efficiency of light as reductor agent wants to be tested, thus two main groups are analysed from this point. These groups are: non borohydride addition and borohydride addition, which serves as an additional reductor agent.

### 4.1.3 Decorated Diatoms - DNA attachment

In order to test viability of diatom frustules as sensor devices, DNA attachment was performed. For this, the dripping method was used, where a drop (approx. 5  $\mu$ L of the final DNA solution was added over solid samples of decorated frustules. This method allows DNA attachment, however, leftovers of probably the elution buffer used in the purification process of DNA, blurred fluorescence microscopy images. Instead, a liquid to liquid mixture of decorated frustules and DNA, shows an observable change in fluorescence, as discussed in the corresponding technique afterwards.

## 4.2 Characterization Au/Ag Nanoparticles

### 4.2.1 UV-Vis Spectroscopy

Diatoms presence needs to be verified. One of the methods used for this purpose, is UV-Vis Spectroscopy. From which, literature reported a peak in the range of 200 to 300 nm for diatoms<sup>94</sup>. In this case, a peak at 254.4 nm shows the presence of Diatoms and confirms its presence after decoration with plasmonic nanoparticles, as shown in Fig. 4.1. Nanoparticles synthesis was developed under two different wavelengths and also two different synthesis methods; one using as a reductor agent just the UV radiation and the other adding sodium borohydride to the synthesis solution under UV radiation. The results are described below.

#### No Borohydride addition

A comparison between the use of blue or green light as reductor is shown in Fig. 4.1 for the in-situ synthesis of Au NPs on top of diatoms, from which a broad peak is shown with a maximum intensity at 528 nm. However, a low intensity peak also appears at 473.8 nm, which might represent a bad distribution in size or change in shape. This is evaluated afterwards with the microscopic techniques.

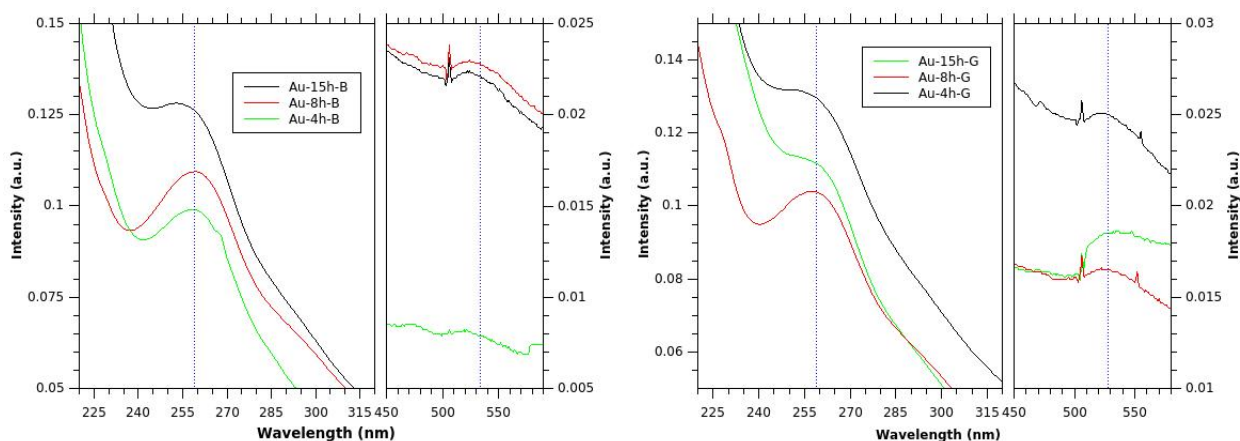


Figure 4.1: UV-Vis spectra from diatoms doped with Au nanoparticles growth under blue light exposure.

Furthermore, there is no observable change in the maximum intensity of Au NPs peak, thus no influence on the wavelength used as a reductor agent for the specific power used. Additionally, the same comparison is shown in Fig. 4.2 for Ag NPs. The same behaviour is observed, since no shift appears from blue to green light as reductor. In this case, the maximum intensity peak corresponding to Ag NPs, is at 525.17 nm.

### Borohydride addition

The same relevant peak confirming the presence of diatoms is shown at 254.4 nm in Fig. 4.3. Here, well defined peaks can be observed for plasmonic nanoparticles and the maximum intensity values have changed with respect to the Not borohydride addition group. Same behaviour can be observed for Ag NPs synthesis, since better defined peaks are shown along with the relevant peak to confirm frustules presence in Fig. 4.4.

In general terms, by using blue light as reductor agent, better defined peaks are shown with respect to the ones synthesised with green light. The peak corresponding to Au NPs here appears at 537.74 nm for blue light, while at 541.935 nm when using green light. A progressive decrease in intensity is observed along the time. For the longest period observed (8h), a slight shift with respect to the others is observed. When using blue light, a redshift appears

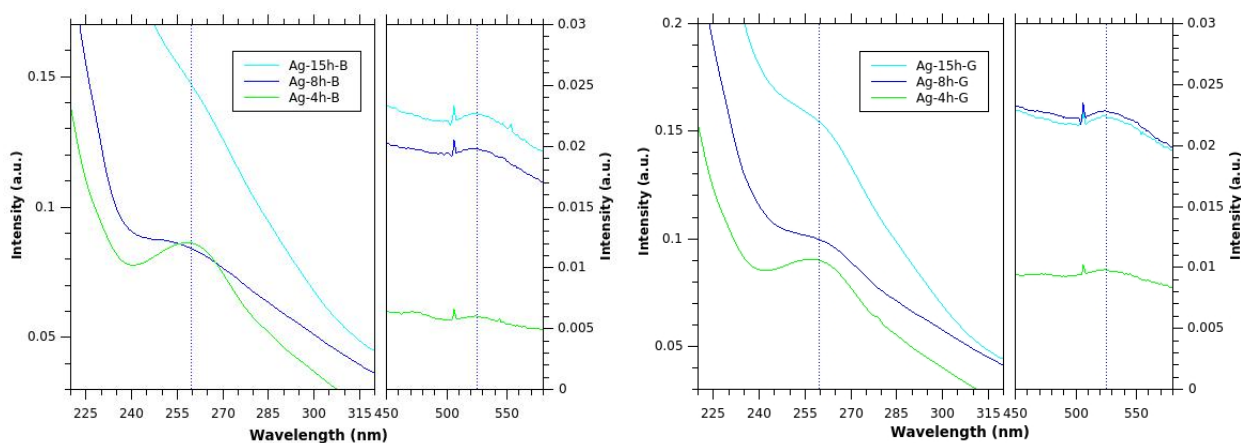


Figure 4.2: UV-Vis spectra from diatoms doped with Ag nanoparticles growth under blue light exposure.

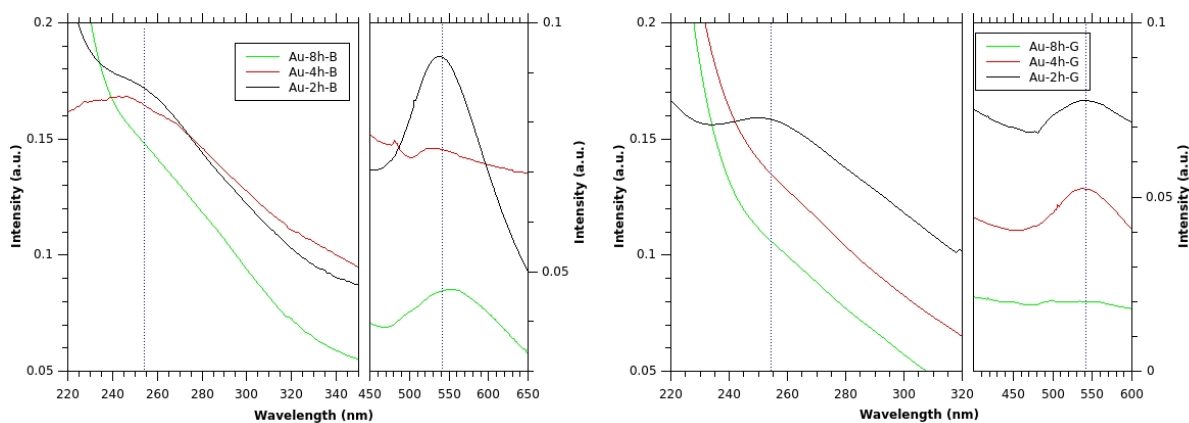


Figure 4.3: UV-Vis spectra from diatoms doped with Au nanoparticles. Borohydride addition (G2).

of about 15 nm, while green light reduction shows a blueshift of about 13 nm. This might show a change in size or even the presence of agglomerates.

Finally, a summary of the maximum intensities of plasmonic nanoparticles in UV-Vis spectra is shown in Table 4.1. No change is observed between green and blue light for the No Borohydride addition, whereas redshift and blueshift appear for Au and Ag NPs respectively in the second group. An increase of Au nanoparticles size with

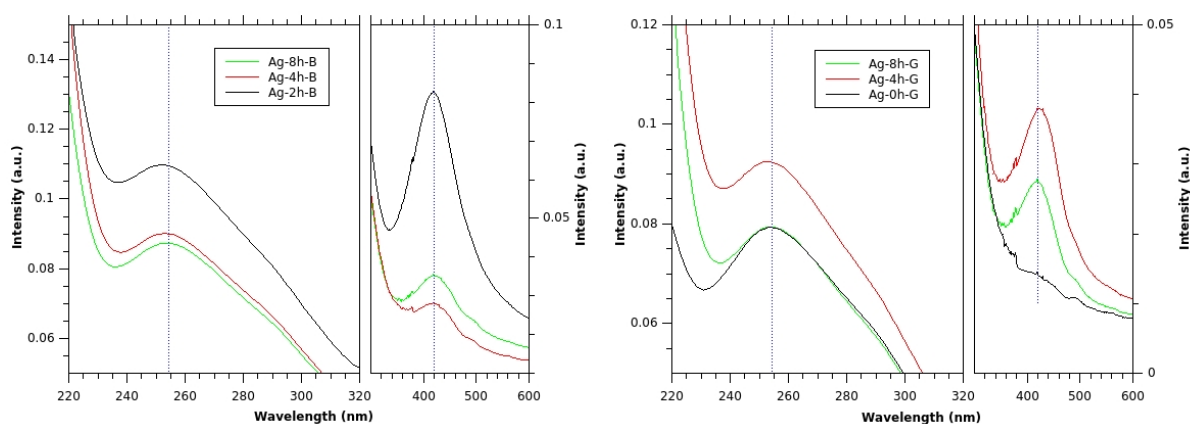


Figure 4.4: UV-Vis spectra from diatoms doped with Ag nanoparticles. Borohydride addition (G2).

increase in absorption peak has been reported in other studies at between 522 and 530 nm<sup>34</sup>. Thus, matching our results with previous works. However, broadness has to be taken in consideration for further size determination since a wide distribution might lead to different average sizes than reported. Furthermore, in-situ synthesis of nanoparticles on top of diatoms has also been performed in other studies, where peptides are used for the synthesis of Ag NPs and highlight their importance to enhance binding ability and photo-induced properties<sup>93</sup>. In this same study, UV-B light is radiated and presence of Ag NPs is confirmed by absorbance spectra in the range between of 400 to 800 nm, as well as the presence of broad peaks which increase their are with time exposure and is assigned to the surface plasmon resonance (SPR) of plasmonic nanoparticles.

Table 4.1: Peak values obtained for both Ag and Au Nanoparticles over diatoms. Here, no shift is observed for NPs synthesis without Borohydride, while a slight shift appears by changing light source in Borohydride addition synthesis.

	Au [nm]		Ag [nm]	
	Blue	Green	Blue	Green
<b>No Borohydride</b>	528	528	525.17	525.17
<b>Borohydride</b>	537.74	541.935	421.93	423.87

### 4.2.2 Scanning Electron Microscopy (SEM)

Diatom frustules chemical composition is mainly Silica. With SEM microscopy, the study of frustules size, qualitative effects of exposure to piranha solution and nanoparticles visualisation was performed. From here, an average size of  $30\ \mu\text{m}$  was obtained of diatom frustules. Besides, a qualitative comparison between the first and second group is shown in 4.5, where the first group (G1) was exposed five days to  $\text{H}_2\text{O}_2$  during the cleaning process and the second group (G2) was exposed to a piranha solution for an hour. Fig. 4.5 shows more incomplete frustule structures for G1 due to the longer exposure time to acid environment, while for G2 complete frustules can be observed, the amount of carbon residues seem to be higher.

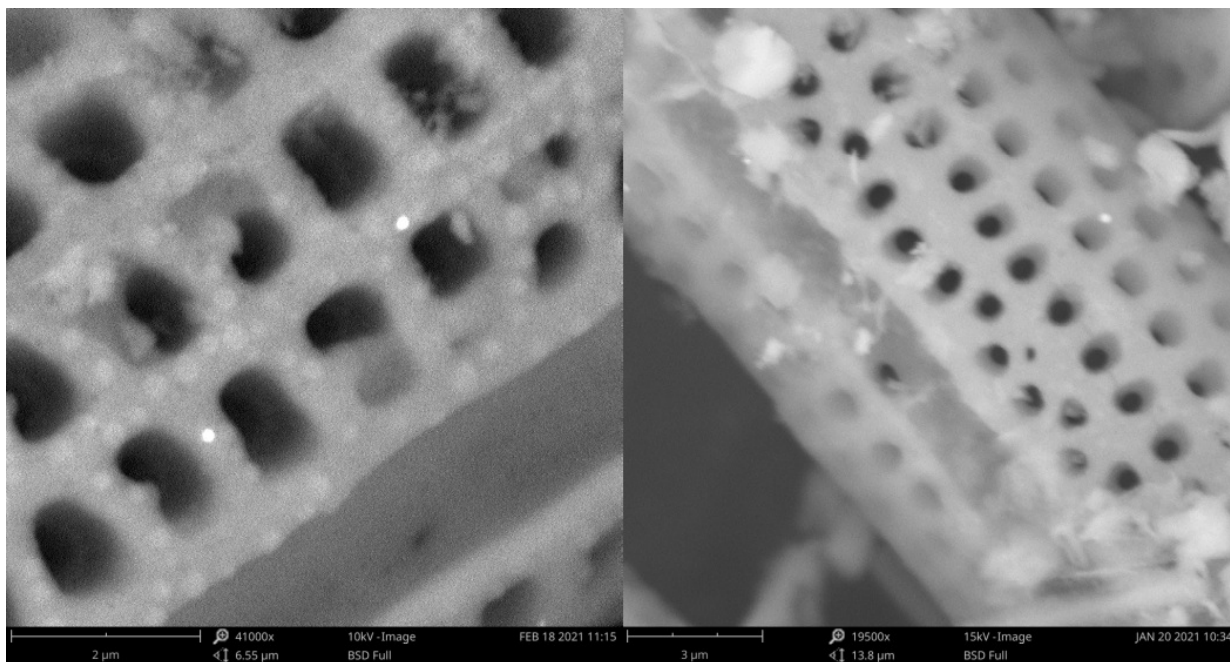


Figure 4.5: SEM comparison of Au NPs frustule decoration under 4h exposure time of Green light from G1 (left) and G2 (right).

On the other hand, nanoparticles size cannot be precisely determined due to the limitations of the equipment. Several dots can be observed along frustule structure and around the pores, thus visual confirmation is achieved. The particles that bring more contrast in the image are the nanoparticles which have a diameter of about  $100\text{nm}$  or more.

---

However, as it will be further observed, by STEM, the size distribution of nanoparticles is smaller and thus appears blurry into the SEM image.

Table 4.2: Nanoparticles average sizes obtained for G1 and G2 (No Borohydride and Borohydride addition respectively) from STEM images.

	No Borohydride (G1)				Borohydride (G2)			
	Au NPs [nm]		Ag NPs [nm]		Au NPs [nm]		Ag NPs [nm]	
	Blue	Green	Blue	Green	Blue	Green	Blue	Green
<b>2H</b>	-	-	-	-	5.64	2.59	17.52	11.44
<b>4H</b>	25.80	63.73	26.45	18.93	2.10	3.20	5.91	14.18
<b>8H</b>	32.23	7.40	12.04	27.60	-	-	-	-

### 4.2.3 Scanning Transmission Electron Microscopy (STEM)

Due to the small sizes of nanoparticles, either a higher resolution microscopy equipment or a transmission electron microscopy is needed. For this reason, Scanning Transmission Electron Microscopy technique, which was available, was used for quantitative nanoparticles size determination and higher resolution imaging.

To this matter, several images were acquired of each sample, further processed and collected to create a distribution plot of nanoparticles size. In Table 4.2 a compilation of the average sizes is shown, divided by the two main groups: non borohydride (G1) and borohydride (G2) addition nanoparticles synthesis, as well as blue and green light exposure. Evolution of average sizes in time, can be observed. On one hand, for G1, an increase in size is observed at blue light for Au NPs and a decrease with green light; while the opposite effect is observed for Ag NPs. On the other hand, for borohydride addition synthesis (G2), Au NPs show a significant decrease in diameter size and the contrary effect than in G1 group. However, this is not conclusive since the change with the time is not significant, while Ag NPs show the same effect as in G1 and also an overall decrease in size.

For the first group, various shapes of nanoparticles were encountered with STEM imaging. Samples were dried from the solution and thus visualised solely and not over diatoms surface. Thus, G1 shows a wide distribution of sizes and shapes, thus the procedure used here might not be accurate in case that specific shapes and sizes are needed. Matching with previous absorption results, Au NPs size is within the error range reported of  $32 \pm 5.4$  nm at

530 nm absorption peak<sup>34</sup>, thus in accordance only for synthesis under blue light exposure. In contrast, the second group showed better sizes distribution and smaller average sizes than the previous group. A better size distribution was expected, since borohydride is a common and well known reductor agent for both Au and Ag NPs synthesis. STEM images were systematically pre-processed and analysed to obtain average sizes from the largest possible amount of nanoparticles visible on each frustule procedure, some of these images are shown in the Appendix section A.3,A.2,A.4,A.5.

Furthermore, from the same equipment, back scattered electrons were also used to acquire a higher compositional contrast image in order to verify Ag and Au nanoparticles sizes on top of diatom frustules. Images were processed and assumed a circular shape in order to calculate an approximate diameter size. Fig. 4.6 shows a comparison of synthesis growth under both blue and green light for 4h light exposure of Au NPs in G2, along with a distribution size plot at the center. With the blue light exposure (upper images) a more defined distribution plot is observed and fitted to a Gaussian function, where its maximum intensity peak is at  $7.14nm$ . In contrast, for green light exposure, the size distribution is less smooth and could even be assigned to two most prominent nanoparticles size. Thus, in the lower side of Fig. 4.6 a size distribution with two peaks is shown with the most recurrent sizes at  $5.4nm$  and  $14.2nm$ .

The same processing of the images was performed for the Ag NPs synthesis. In contrast to Au NPS, a smoother transition of size distribution appears for Ag NPs with two most recurrent sizes, observed in Fig. 4.7. Blue light exposure (upper images) shows a size distribution with the most recurrent size at  $1.7nm$  and a less recurrent size at  $10.2nm$ . On the other side, a more defined size is observed at  $3.8nm$  and the significantly less recurrent size at  $10nm$  for green light exposure (lower images). Here, the change in light exposure wavelength seems to promote the synthesis of smaller sized nanoparticles.

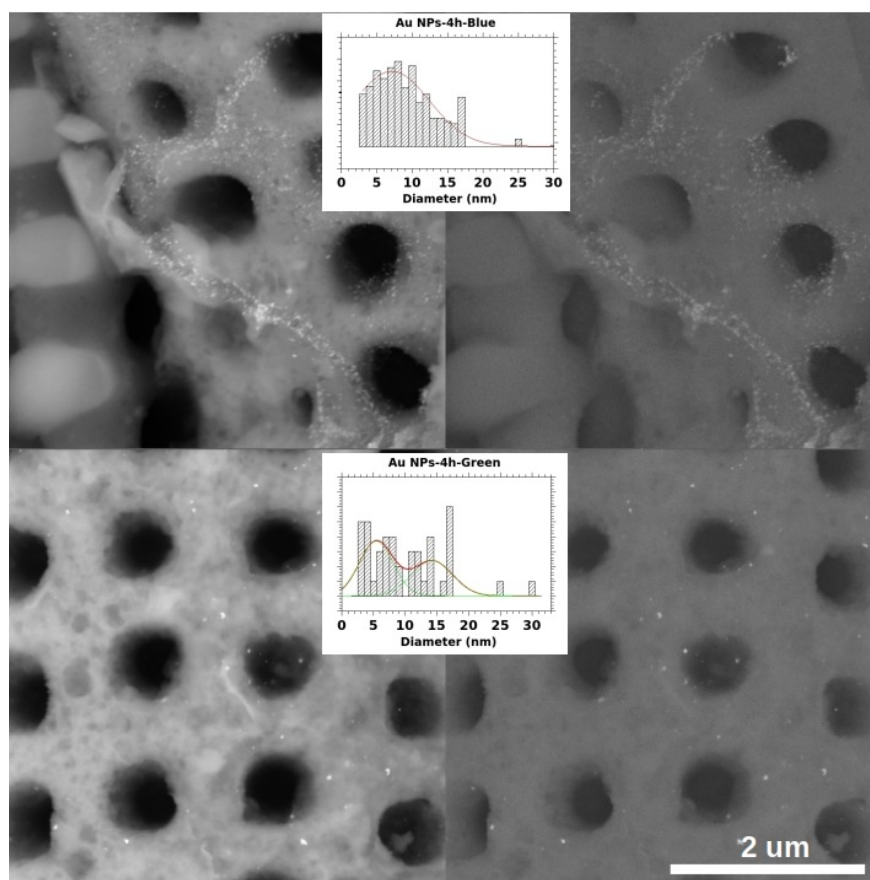


Figure 4.6: Back scattered electron (BSE) (left) and In-beam BSE (right) images from G2 diatom frustules decorated with Au NPs of 4h exposure to blue (upper) and green (lower) light exposure. Images were taken at 10 kV, view field of 4.46  $\mu\text{m}$ , magnification of 155 kx and working distance of 10.01 mm with back scattered electrons.

#### 4.2.4 Raman Spectroscopy

Along this study, plasmonic nanoparticles have been used, which in several studies have proved of benefit for raman signal acquisition. By literature review, it is known that diatoms frustules have fluorescence with no need of further functionalisation. This is a problem when acquiring raman spectra due to the high background obtained, thus avoiding the visualisation of Raman signal<sup>96</sup>. However, Surface Enhanced Raman Spectroscopy (SERS) is a technique which uses plasmonic nanoparticles to enhance the signal of, for example, organic molecules. The same principle then, is applied here, since both Ag and Au NPs are covering diatoms frustules, causing its localised plasmon effect

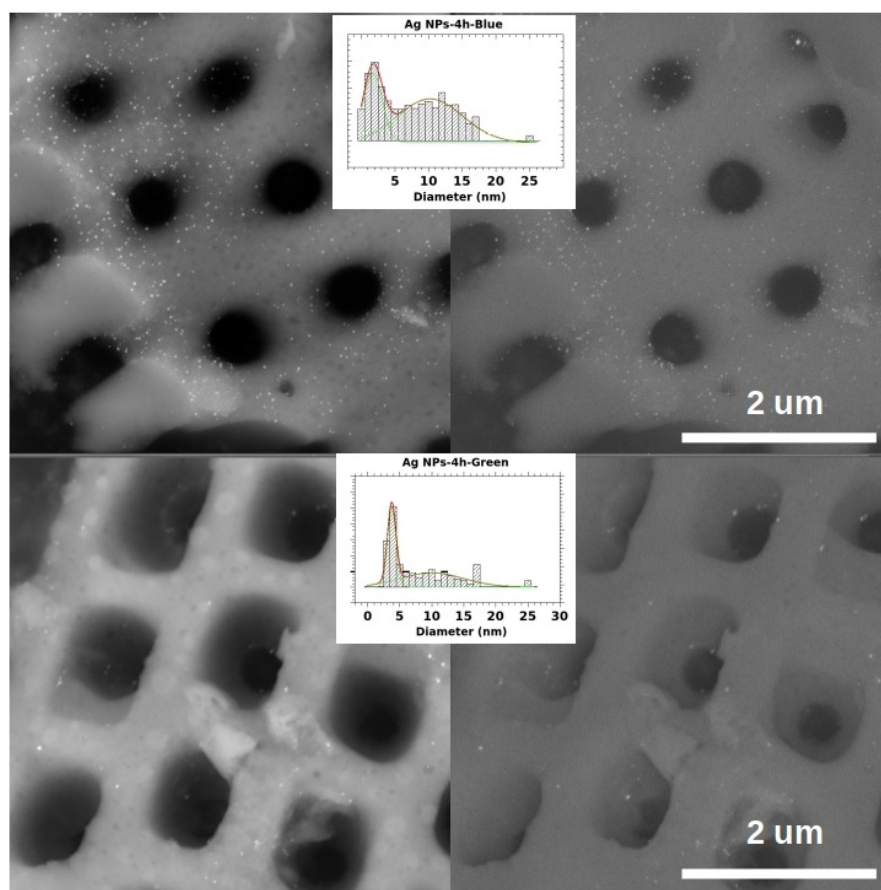


Figure 4.7: Back scattered electron (BSE) (left) and In-beam BSE images from G2 diatom frustules decorated with Ag NPs of 4h exposure to blue (upper) and green (lower) light exposure. Images were taken at 10 kV, view field of 4.46  $\mu\text{m}$ , magnification of 155 kx, with back scattered electrons and working distance of 9.94 mm (upper) and 10.01 mm (lower).

to enhance frustules signal.

In Fig. 4.8 a comparative analysis is shown, between two different excitation wavelengths that were used to obtain raman signal of frustules decorated with Ag NPs. Additionally, the evolution of raman spectra with exposure time during synthesis of NPs is shown. In general terms, fluorescence background is observed for both excitation wavelengths at 2 and 8 hours to light exposure and broad peaks at about 1600 and 2800  $\text{cm}^{-1}$ , while for frustules of

4 hours exposure to light, better defined peaks are shown. In comparison, higher wavelength excitation for raman signal acquisition, decreases fluorescent background. The source of fluorescence comes from carotenoids present in diatom frustules, which absorption spectra goes from 460 to 530 nm approximately, thus in the range of resonance shown in raman spectra<sup>96,101,102</sup>.

The most relevant peaks could be the ones at  $1000\text{ cm}^{-1}$  most probably corresponding to  $\nu\text{C-C}$  gauche vibration coming from carbon residuals, at  $1304$  and  $1440\text{ cm}^{-1}$  from  $\delta\text{CH}_2$  twisting and scissor respectively, corresponding to the cylindrical structure of the frustule and further confirmed by FTIR spectra in the coming sections. Finally, at  $1660\text{ cm}^{-1}$  from  $\nu\text{C=C}$  cis, as mentioned by Meksiarun (2012)<sup>96</sup> or even the source of fluorescence that could be chlorophyll-a or b. However, luminescence background along the spectrum is not clearly defined and thus several other spectra were acquired at different conditions before obtaining this last one. Some of those were to place the sample on carbon, glass and silicon holders. Besides, ambient light was not a critical source of luminescence were turned off and no improvements were observed. In conclusion, spectra was acquired by placing decorated diatoms with and without DNA over a silicon surface, while taking care no other light source than the equipment is affecting the spectra. As an initial hypothesis, we believe the sinusoidal noise at the spectra is due to the frustule structure and fine inner pore sizes that somehow encapsulates certain amount of luminescence from the spectrometer laser itself. A reference spectra is shown in Fig. 3.6 at the lower right side, but since diatom frustules have a variety of shapes and structures, only certain peaks could be compared with the present study.

Measuring conditions for all spectra were acquired with a 100X augment lense, and 15 seconds of time exposure. Relative power of 1% equal to 16.2 mW was used for the 633nm wavelength, while a relative power of 1% equal to 51.3 mW for the 532 nm wavelength. Furthermore, peaks at  $240$  and  $1010\text{ cm}^{-1}$  are representative of Ag NPs, as mentioned by VanderHorst<sup>103</sup> and Ramirez<sup>104</sup>. This is also observed in our reference spectra within Fig. 3.6 at the top right corner, where the peak around  $240\text{ cm}^{-1}$  might be attributed to the  $\nu\text{Ag} - \text{OCO}^{-1}$  vibrations. The latter is a representative peak since looking at Fig.4.9 right side, a significant change in intensity is observed after DNA addition, and a better visualization of raman signals thus representing an important feature for biosensing purposes to investigate more in-depth.

After the latter analysis concerning time exposure during synthesis of nanoparticles, the best spectra appeared at

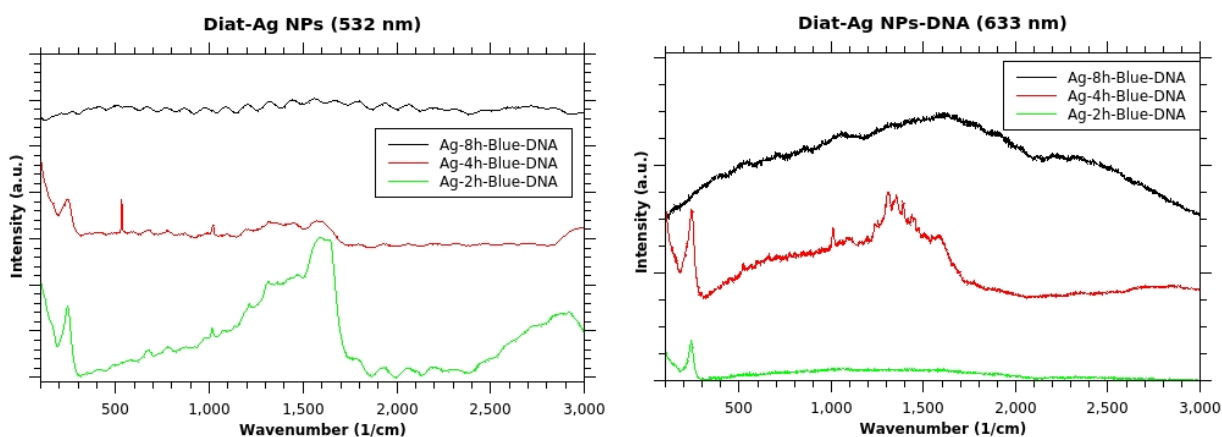


Figure 4.8: Raman spectra at two different excitation wavelengths from Ag NPs decorated diatoms with DNA attachment.

4 hours exposure, which along with NPs sizes in electron microscopy, has the best distribution and less spread sizes on diatom frustules. Thus, more in-depth analysis is performed for sensing purposes. From here, a spectra was taken before and after DNA attachment. In general, an increase in signal intensity is shown after DNA attachment, serving the purpose of a sensor. However, in the case of Au decorated frustules, there is no observable raman peaks due to the before analysed fluorescence background. Thus, it is inferred that, most probably, the quantity of nanoparticles synthesised on frustules surface was not enough hence higher wavelength excitation laser should be used to acquire raman signal.

In contrast, Ag NPs already showed observable raman peaks at least for the 4h time exposure. Correlating these results with nanoparticles size, Ag NPs show the higher average size with green light at 4h in G2, converting this as the best option for sensor testing purposes concerning raman signal. Hence, Fig. 4.9 shows again a comparison between the use of 532 and 633 nm wavelengths for this specific decoration process. In both cases, a low intensity spectra appears before DNA attachment with broad peaks, while after DNA attachment intensity signal increases. Better defined peaks are shown after DNA binding, however a stronger background noise appears at 633 nm. This could be assigned to a shift in the absorbance peak of frustules along with DNA.

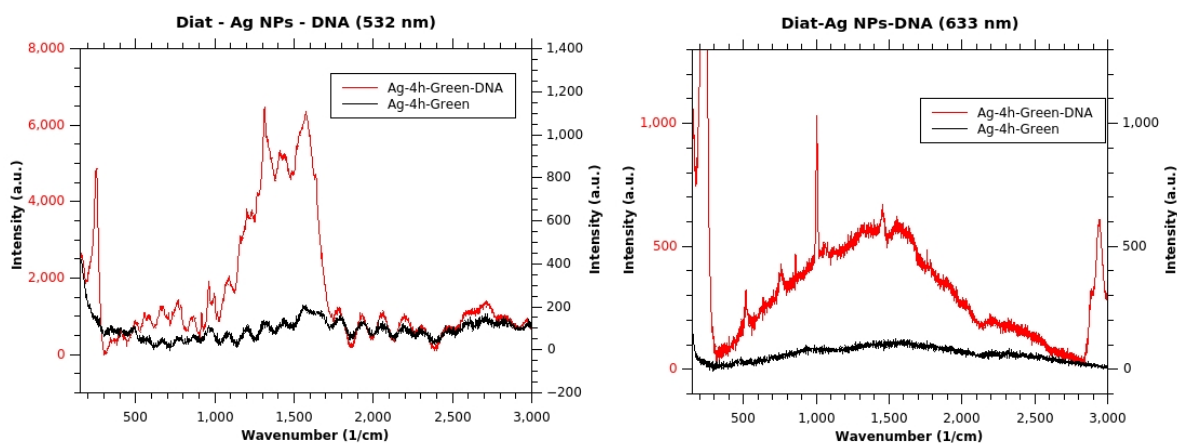


Figure 4.9: Raman spectra at two different excitation wavelengths from Ag NPs with 4 hours of light exposure during the synthesis, on top of diatoms with DNA attachment.

### 4.2.5 Fluorescence Microscopy

By using different light sources, it was possible to identify nanoparticles on top of diatom frustules, as well as to observe the change in light emission before and after DNA attachment, as shown in 4.10. Due to surface plasmon resonance it is possible to observe nanoparticles by image contrast on top of diatoms even if the microscope resolution is not as high to observe them directly. From the previous analysis, higher fluorescence background was observed for Au NPs at the used excitation wavelengths, thus for fluorescence microscopy sensing purposes Au decorated frustules were chosen for detailed experimentation. More specifically, Au decorated frustules with 4 hours to blue light exposure were further analysed.

Fluorescence was tested for both blue and green light, however no significant changes were observed under green light. Diatom frustules themselves are fluorescent, as shown in Fig. 4.10-b where emission at  $492\text{nm}$  is observed, while after DNA attachment, an emission light with maximum intensity at around  $468\text{nm}$  appears. Thus, DNA attachment induces a shift in emission wavelength under blue light exposure, useful as a sensor feature. However, this effect was observed only for Au decorated frustules with 4 hours exposure to blue light from the second group. As mentioned by Villani<sup>98</sup>, diatoms themselves have their inner fluorescence and can be further enhanced by the

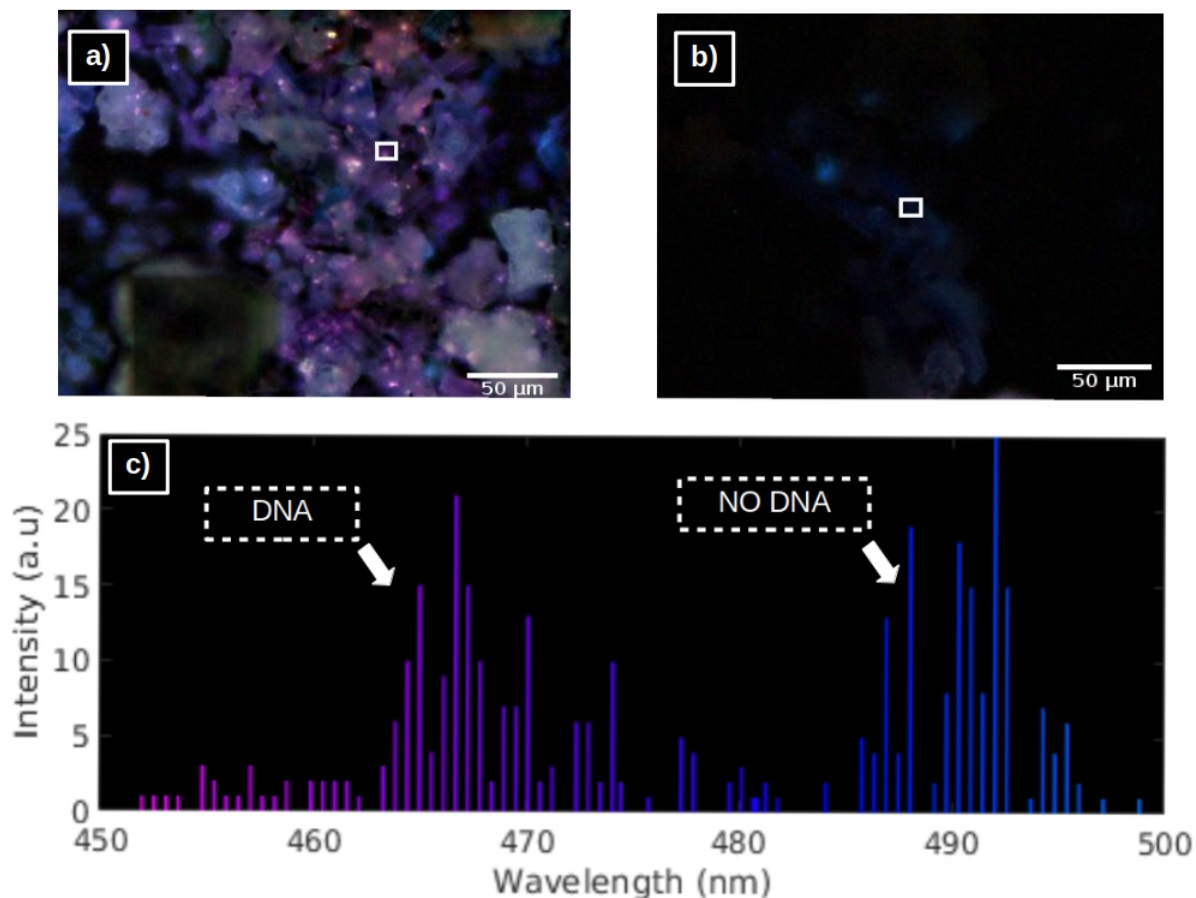


Figure 4.10: Diatom frustules observed with the fluorescence microscopy mode on blue light. Here, from G2, diatoms decorated with Au NPs under 4h exposure to blue light is shown, where a) DNA doped frustules, b) Non-DNA doped frustules and c) is the emission wavelength of a,b images.

addition of fluorescent molecules or plasmonic nanoparticles in this case. Fig. 3.9 shows an example of fluorescence imaging of diatoms where the full structures can be observed emitting. However, for comparison purposes RGB colors from image were converted to approximate wavelength. The code used to transform from RGB colours to wavelength, is shown in the Appendix section. Fluorescence imaging was performed on decorated frustules before and after DNA binding, showing poor or none effect when DNA was placed directly on top of dried decorated

frustules.

#### 4.2.6 Fourier Transform Infrared Spectroscopy (FTIR)

In order to determine the composition of the sample, DNA attachment and to identify certain bonds, FTIR technique is applied and shown in Fig. 4.11. Initially, one of the most prominent peaks at around  $1003\text{ cm}^{-1}$ , corresponding to Si-O stretching, Si-OH and Si-O-Si siloxane group due to the frustules from Diatoms. This is connected to the peaks at about  $1408\text{ cm}^{-1}$  corresponding to C=O carboxyl group stretching vibration, most probably due to the remaining of carbonates left over the sample even after the acid treatment; and the following peak at  $1440\text{ cm}^{-1}$  assigned to carbonates as well, that disappear in the already decorated diatom spectra. Besides, into the footprint zone of the FTIR spectra ( $400\text{-}800\text{ cm}^{-1}$ ), peak at  $791\text{ cm}^{-1}$  corresponding to Si-O silanol stretching in diatoms, as well as peak at  $444\text{ cm}^{-1}$  most probably corresponding to siloxane bending. A similar study was made by Alipour<sup>100</sup> where Si-O bonding range corresponds with results in this study. Moreover, to identify DNA by FTIR, Taboury<sup>99</sup> gives a detailed description of DNA molecular compounds, which are correlated here. Both DNA and diatoms reference spectra can be observed in Fig.3.10 for better comparison.

Furthermore, at  $1644\text{ cm}^{-1}$  there are different interpretations that can be proposed, similar to Mazumder et al. (2014)<sup>105</sup>, namely:

- *N-H* bondings and stretching associated to amine groups, which since it stands along the evolution of samples, it might correspond to silaffin structures, responsible for hierarchical organisation in diatoms<sup>106</sup>.
- *H-O-H* bending of adsorbed water necessary for nanoparticles reduction.
- *Si-OH* stretching mostly due to the acid piranha treatment on diatoms.

Finally, the broad peak at  $3433\text{ cm}^{-1}$  which corresponds to hydroxyl groups is probably due to bond water surface. However, an important contribution includes Si-OH stretching mode in frustules, mentioned before by Gale(2009)<sup>105,107</sup>.

From Fig. 4.11 it is possible to compare the use of blue (463 nm) and green (511 nm) light as reductor agent. Observing the most prominent peak at  $1040.5\text{ cm}^{-1}$  and shoulder at  $1086\text{ cm}^{-1}$ , corresponding to deoxyribose and

$PO_2^-$  stretching<sup>99</sup>. Thus, knowing they are linked to DNA attachment, a progressive increase in absorption is seen along with the increase in exposure time to the blue light. In contrast, with the green light a decrease in absorption is observed. This might show that more energetic light sources allow a progressive size modification of nanoparticles and thus an increase in DNA molecules attached to the structure.

On the other hand, Fig. 4.12 shows FTIR spectra for Ag NPs decoration on diatoms with the use of blue light as reductor. A decrease in the same peak at  $1040.5\text{ cm}^{-1}$  is observed, opposite to what is shown for Au NPs doped diatoms, supported by the change in  $3367\text{ cm}^{-1}$  with also a decrease. Additionally, the right hand figure shows a similar spectrum for 2h exposure with green light, which might suggest a poor synthesis of Ag NPs on top of diatoms.

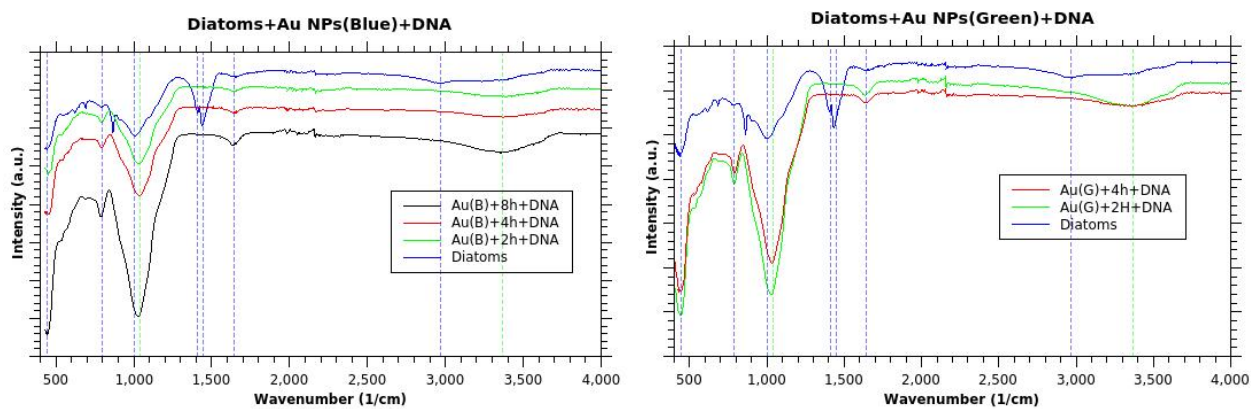


Figure 4.11: FTIR spectra from Diatoms alone and after Au NPs decoration along with DNA attachment. Green lines correspond to peaks appearing only after DNA addition, while blue lines are peaks present in raw diatoms. Left and right figures correspond to blue and green light as reductor agent, respectively.

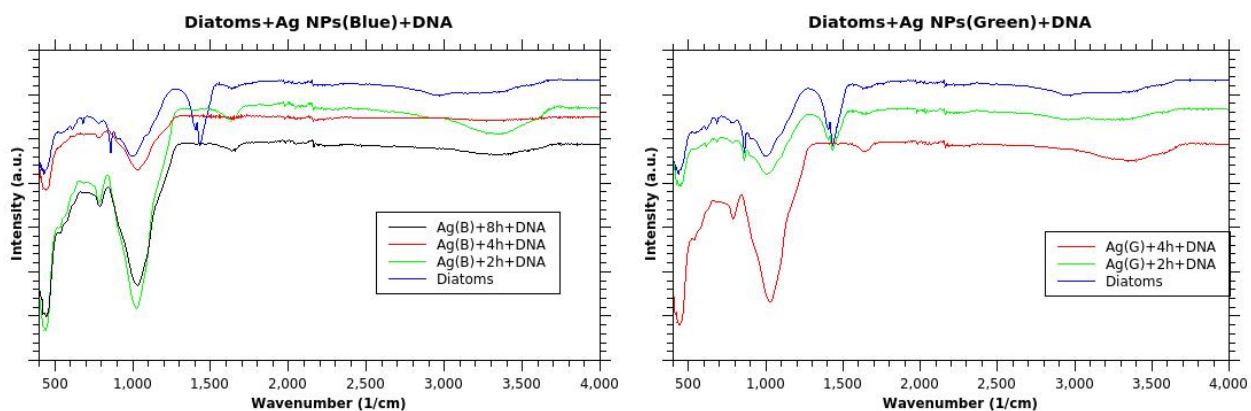


Figure 4.12: FTIR spectra from Diatoms alone and after Ag NPs decoration along with DNA attachment. Left and right figures correspond to blue and green light as reductor agent, respectively, showing an opposite behaviour than Au doped NPs.

## Chapter 5

# Conclusions & Outlook

Frustules decoration was initially tested by UV-Vis Spectroscopy, from which the presence of both Ag and Au NPs was confirmed. These results match with further image analysis performed by STEM technique where two most recurrent sizes were assigned and a compilation of average sizes for G1 and G2 groups to check their evolution with light exposure time. Furthermore, the effect of acid treatment on diatom frustules was observed under SEM imaging where extended time exposure destroys their structure but also eliminates carbon residuals. Group 2 showed better defined nanoparticle sizes and thus more in depth analysis was performed here. Raman analysis of G2 checked the effect of Ag and Au NPs on frustules signal, where Au NPs had too much fluorescence background and Ag NPs performs better for assigning certain peaks corresponding to nanoparticles and frustules. The effect of excitation for Raman signal was also tested, where higher wavelengths offer better resolution of Raman peaks. Time of 4 hours exposure to either blue or green light during the synthesis process, appears as the best time taking into account size distribution, shape and recurrence of nanoparticles, as well as raman signal. From here, this exposure time is only considered for further analysis. Fluorescence analysis was used to confirm the high fluorescence effect of Au NPs, where a shift in the wavelength emission is observed after DNA binding, with similar effect in raman spectroscopy on Ag NPs. Finally, attaching of DNA to decorated frustules was followed by the FTIR technique by checking absorbance intensity, where an increase in absorbance is observed. Au NPs show a better attachment to DNA under blue light exposure during the synthesis, while Ag NPs has a more favorable attachment under green light exposure.

In conclusion, time exposure of 4h to light appears as the best procedure in matters of defined shape and size of NPs. Ag NPs show a better performance under green light exposure and the best option for sensing under raman

spectroscopy, while Au NPs outstand their performance under blue light exposure for sensors with fluorescence effect. Diatom frustules have shown to be an adequate template for plasmonic decoration and further use for sensing purposes. However, for tunability of size, shape of NPs and thus plasmonic effects, further studies need to be performed, from which we recommend, factors such as stirring frequency during synthesis, DNA attachment and power of light source to be further analysed, along with a detailed raman analysis that includes mapping of the full sample.

## Appendix A

# Long Appendix 1 Heading

This is the code used to estimate RGB colours to wavelength with Matlab.

```
1 clear;clc;
2
3 rgbImage= importdata('Image_3166-2ROI.tif');
4 rgbImage1=importdata('Image_3248-2ROI.tif');
5
6 hsvImage = rgb2hsv(rgbImage); % Convert the image to HSV space
7 hPlane = 360.*hsvImage(:, :, 1); % Get the hue plane scaled from 0 to 360
8
9 binEdges = 0:300; % Edges of histogram bins
10 N = histc(hPlane(:), binEdges); % Bin the pixel hues from above
11 wavelength = 620-(170/300).*(0:299); % Approximate wavelength
12
13 hsvImage1 = rgb2hsv(rgbImage1); % Convert the image to HSV space
14 hPlane1 = 360.*hsvImage1(:, :, 1); % Get the hue plane scaled from 0 to 360
15
16 N1 = histc(hPlane1(:), binEdges); % Bin the pixel hues from above
17
18 y=[N(1:end-1) N1(1:end-1)];
19 hBar = bar(wavelength,y, 'histc'); % Plot the histogram
20
21 set(hBar, 'CData', 300:-1:1, ... % Change the color of the bars using
22 'CDataMapping', 'direct',... % indexed color mapping (360 colors)
```

```
23     'EdgeColor','none');           % and remove edge coloring
24 colormap(hsv(360));               % Change to an HSV color map with 360 points
25 axis([450 500 0 max(N)]);         % Change the axes limits
26 set(gca, 'Color', 'k');            % Change the axes background color
27 set(gcf, 'Pos', [50 400 560 200]); % Change the figure size
28 xlabel('Wavelength (nm)');        % Add an x label
29 ylabel('Intensity (a.u)');        % Add a y label
```

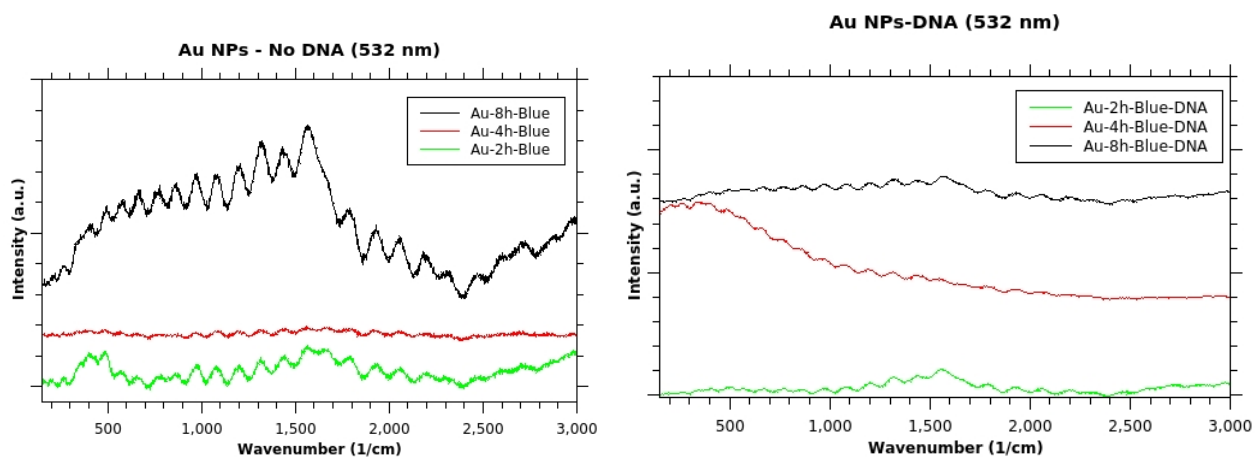


Figure A.1: Raman spectra intensity increase before and after DNA attachment to Au decorated diatoms. Au NPs here were exposed for 4 hours to blue light during synthesis. No well defined Raman signal observed for Au decorated diatoms.

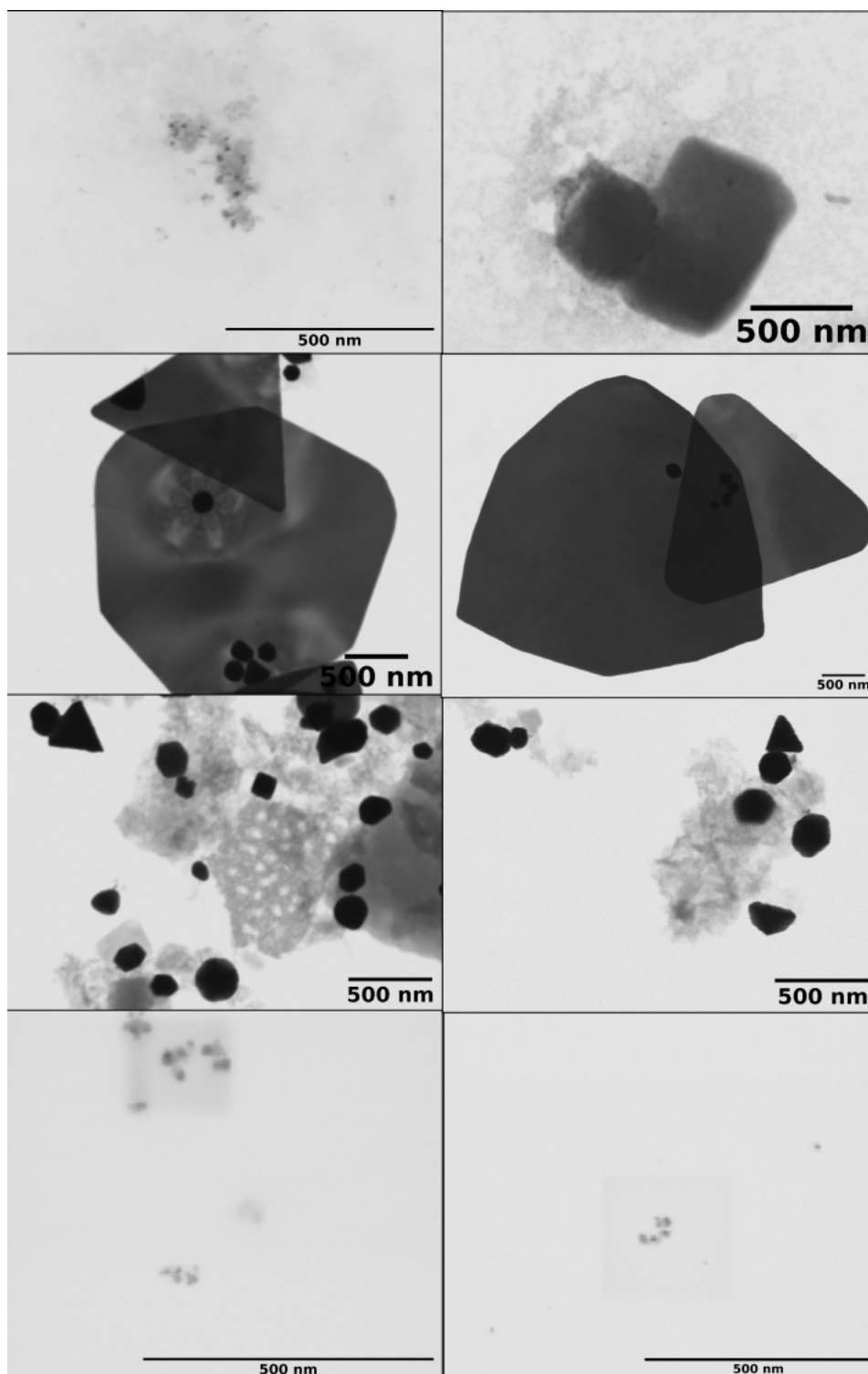


Figure A.2: Acquired STEM images for G1 Au NPs, which were included to pre-process and calculate nanoparticles diameter sizes. Rows correspond to: 1) Au-4h-Blue, 2) Au-4h-Green, 3) Au-8h-Blue, 4) Au-8h-Green.

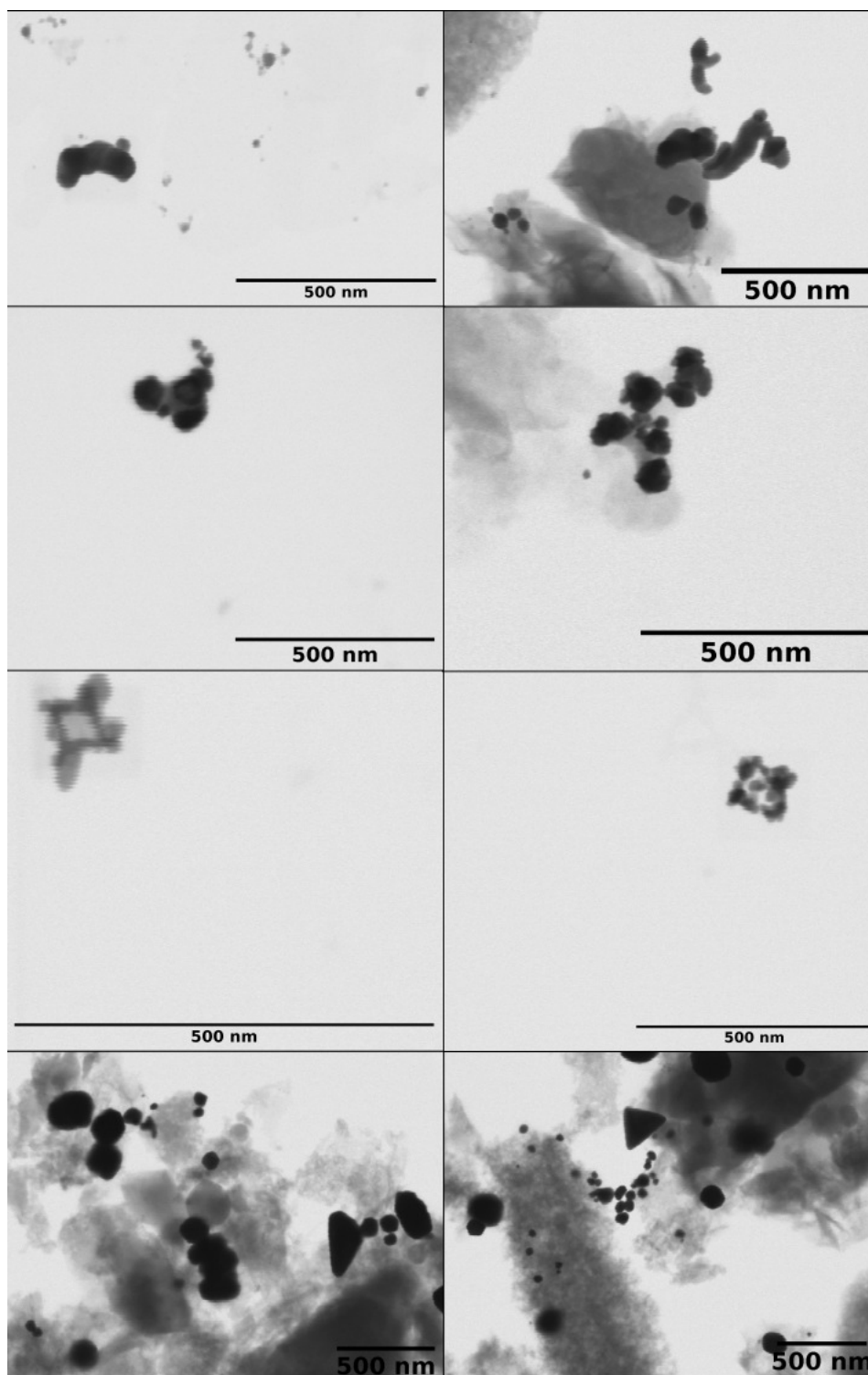


Figure A.3: These are the acquired STEM images for G1 Ag NPs, which were included to pre-process and calculate nanoparticles diameter sizes. Rows correspond to: 1) Ag-4h-Blue, 2) Ag-4h-Green, 3) Ag-8h-Blue, 4) Ag-8h-Green.

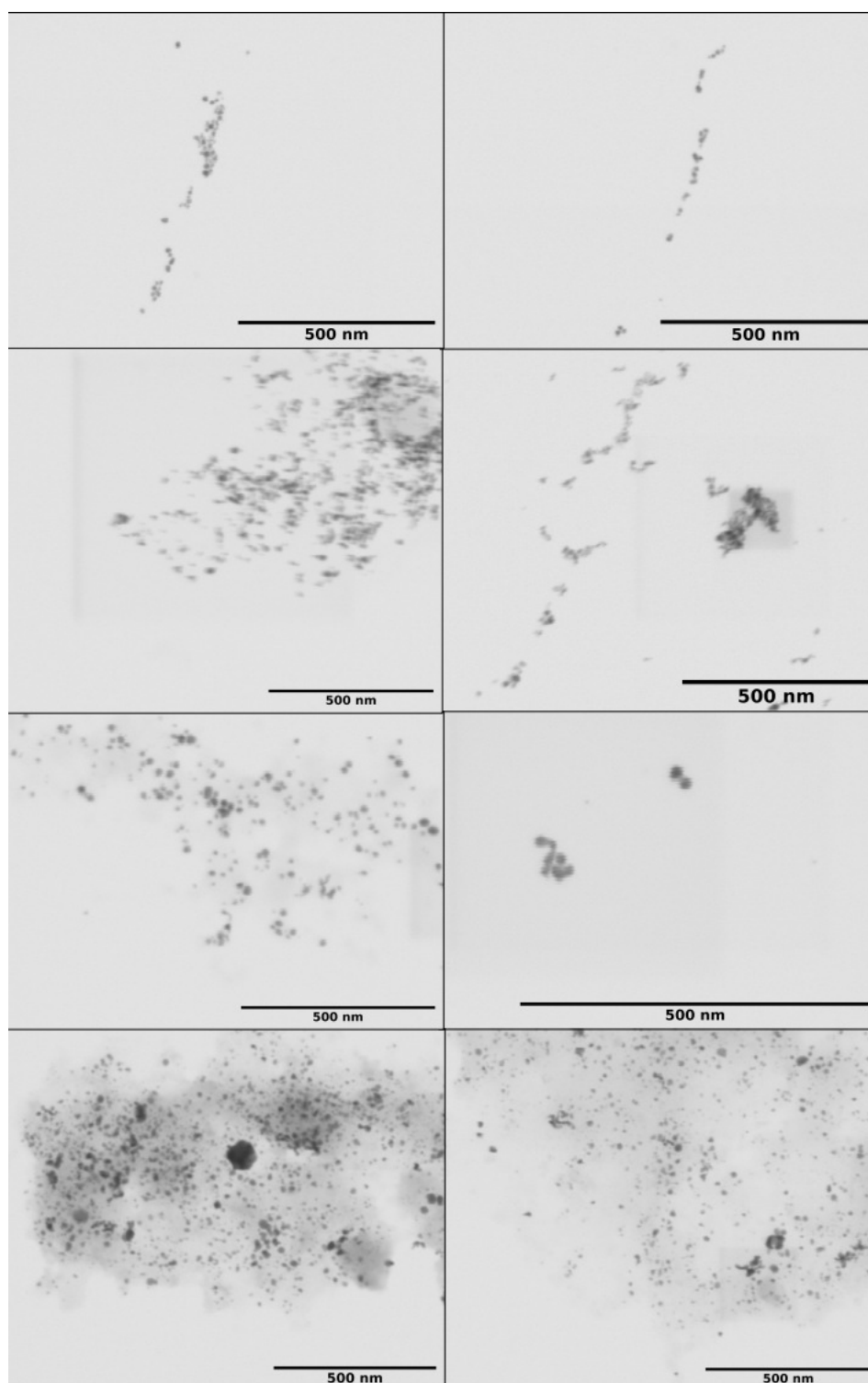


Figure A.4: These are the acquired STEM images for G2 Au NPs, which were included to pre-process and calculate nanoparticles diameter sizes. Rows correspond to: 1) Au-2h-Blue, 2) Au-2h-Green, 3) Au-4h-Blue, 4) Au-4h-Green.

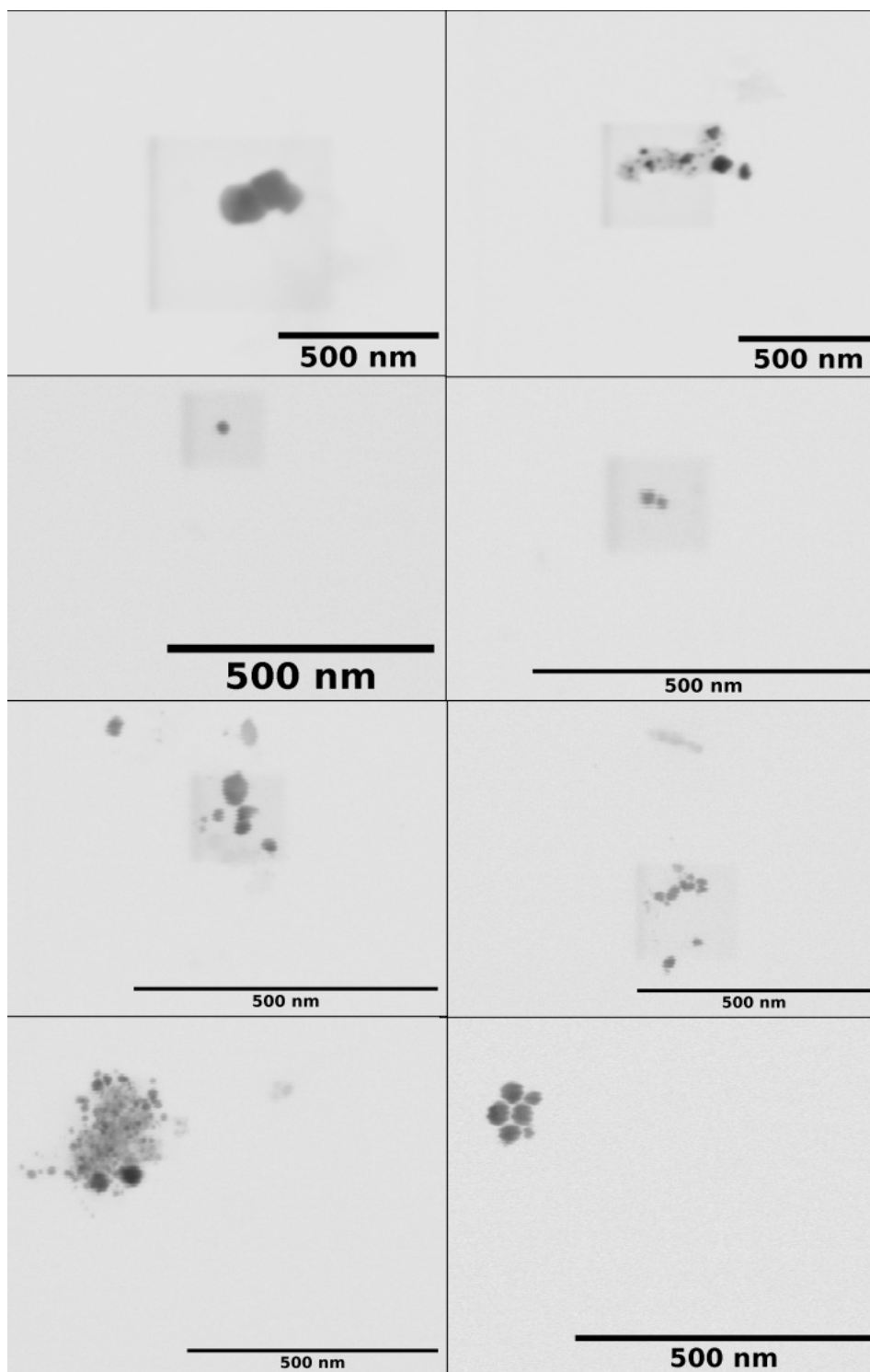


Figure A.5: These are the acquired STEM images for G2 Ag NPs, which were included to pre-process and calculate nanoparticles diameter sizes. Rows correspond to: 1) Ag-2h-Blue, 2) Ag-2h-Green, 3) Ag-4h-Blue, 4) Ag-4h-Green.



# Bibliography

- [1] Rogato, A.; Tommasi, E. D. Physical, Chemical, and Genetic Techniques for Diatom Frustule Modification: Applications in Nanotechnology. *Applied Sciences* **2020**, *10*, 8738.
- [2] Saad, E. M.; Pickering, R. A.; Shoji, K.; Hossain, M. I.; Glover, T. G.; Krause, J. W.; Tang, Y. Effect of cleaning methods on the dissolution of diatom frustules. *Marine Chemistry* **2020**, *224*, 103826.
- [3] Gholami, P.; Khataee, A.; Bhatnagar, A. Environmentally superior cleaning of diatom frustules using sono-Fenton process: Facile fabrication of nanoporous silica with homogeneous morphology and controlled size. *Ultrasonics Sonochemistry* **2020**, *64*, 105044.
- [4] Ren, F.; Campbell, J.; Wang, X.; Rorrer, G. L.; Wang, A. X. Enhancing surface plasmon resonances of metallic nanoparticles by diatom biosilica. *Optics Express* **2013**, *21*, 15308.
- [5] Pacifici, D.; Lezec, H. J.; Sweatlock, L. A.; Walters, R. J.; Atwater, H. A. Universal optical transmission features in periodic and quasiperiodic hole arrays. *Optics Express* **2008**, *16*, 9222.
- [6] Kong, X.; Li, E.; Squire, K.; Liu, Y.; Wu, B.; Cheng, L.-J.; Wang, A. X. Plasmonic nanoparticles-decorated diatomite biosilica: extending the horizon of on-chip chromatography and label-free biosensing. *Journal of Biophotonics* **2017**, *10*, 1473–1484.
- [7] Setaro, A.; Lettieri, S.; Maddalena, P.; Stefano, L. D. Highly sensitive optochemical gas detection by luminescent marine diatoms. *Applied Physics Letters* **2007**, *91*, 051921.
- [8] Lyddy, R. *Information Resources in Toxicology*; Elsevier, 2009; pp 321–328.
- [9] Booth, T.; Baker, M. *Pharmacognosy*; Elsevier, 2017; pp 633–643.

- [10] Khan, I.; Saeed, K.; Khan, I. Nanoparticles: Properties, applications and toxicities. *Arabian Journal of Chemistry* **2019**, *12*, 908–931.
- [11] AlKahtani, R. N. The implications and applications of nanotechnology in dentistry: A review. *The Saudi Dental Journal* **2018**, *30*, 107–116.
- [12] Liu, L.; Xi, N.; Li, G.; Chen, H. *Nano Optoelectronic Sensors and Devices*; Elsevier, 2012; pp 51–79.
- [13] Hobson, D. *Comprehensive Biotechnology*; Elsevier, 2011; pp 683–697.
- [14] Pokropivny, V.; Skorokhod, V. Classification of nanostructures by dimensionality and concept of surface forms engineering in nanomaterial science. *Materials Science and Engineering: C* **2007**, *27*, 990–993.
- [15] Malhotra, B. D.; Ali, M. A. *Nanomaterials for Biosensors*; Elsevier, 2018; pp 1–74.
- [16] Asha, A. B.; Narain, R. *Polymer Science and Nanotechnology*; Elsevier, 2020; pp 343–359.
- [17] Neikov, O. D.; Yefimov, N. A. *Handbook of Non-Ferrous Metal Powders*; Elsevier, 2019; pp 271–311.
- [18] Sharma, P.; Brown, S.; Walter, G.; Santra, S.; Moudgil, B. Nanoparticles for bioimaging. *Advances in Colloid and Interface Science* **2006**, *123-126*, 471–485.
- [19] Li, H.; Jiao, J.; Campbell, J.; Rorrer, G. L.; Jiang, B.; Liu, Y.; Wang, R. Novel form of photonic crystals for bioimaging contrast enhancement. 2011; <https://doi.org/10.1109/cisp.2011.6100347>.
- [20] Thévenot, D. R.; Toth, K.; Durst, R. A.; Wilson, G. S. Electrochemical biosensors: recommended definitions and classification. International Union of Pure and Applied Chemistry: Physical Chemistry Division, Commission I.7 (Biophysical Chemistry) Analytical Chemistry Division, Commission V.5 (Electroanalytical Chemistry).1. *Biosensors and Bioelectronics* **2001**, *16*, 121–131.
- [21] *Advanced Nanomaterials for Solar Cells and Light Emitting Diodes*; Elsevier, 2019.
- [22] Brocke, T. *Electronic Raman spectroscopy on semiconductor quantum dots : dissertation : zur Erlangung des Doktorgrades des Departements Physik der Universität Hamburg*; Cuvillier Verlag: Gottingen Germany, 2007.
- [23] Sprynskyy, M.; Pomastowski, P.; Hornowska, M.; Król, A.; Rafińska, K.; Buszewski, B. Naturally organic functionalized 3D biosilica from diatom microalgae. *Materials & Design* **2017**, *132*, 22–29.

- [24] Sanderson, M. J.; Smith, I.; Parker, I.; Bootman, M. D. Fluorescence Microscopy. *Cold Spring Harbor Protocols* **2014**, 2014, pdb.top071795–pdb.top071795.
- [25] Hegyi, J.; Hegyi, V. *Imaging in Dermatology*; Elsevier, 2016; pp 89–94.
- [26] Dugdale, R. C.; Wilkerson, F. P. Silicate regulation of new production in the equatorial Pacific upwelling. *Nature* **1998**, 391, 270–273.
- [27] Cullis, A. G.; Canham, L. T.; Calcott, P. D. J. The structural and luminescence properties of porous silicon. *Journal of Applied Physics* **1997**, 82, 909–965.
- [28] Rea, I.; Terracciano, M.; Stefano, L. D. Synthetic vs Natural: Diatoms Bioderived Porous Materials for the Next Generation of Healthcare Nanodevices. *Advanced Healthcare Materials* **2016**, 6, 1601125.
- [29] Stoermer, E. F., Smol, J. P., Eds. *The Diatoms*; Cambridge University Press, 1999.
- [30] Onesto, V.; Villani, M.; Coluccio, M. L.; Majewska, R.; Alabastri, A.; Battista, E.; Schirato, A.; Calestani, D.; Coppedé, N.; Cesarelli, M.; Amato, F.; Fabrizio, E. D.; Gentile, F. Silica diatom shells tailored with Au nanoparticles enable sensitive analysis of molecules for biological, safety and environment applications. *Nanoscale Research Letters* **2018**, 13.
- [31] Losic, D.; Mitchell, J. G.; Voelcker, N. H. Diatomaceous Lessons in Nanotechnology and Advanced Materials. *Advanced Materials* **2009**, 21, 2947–2958.
- [32] Ferrara, M. A.; Dardano, P.; Stefano, L. D.; Rea, I.; Coppola, G.; Rendina, I.; Congestri, R.; Antonucci, A.; Stefano, M. D.; Tommasi, E. D. Optical Properties of Diatom Nanostructured Biosilica in *Arachnoidiscus* sp: Micro-Optics from Mother Nature. *PLoS ONE* **2014**, 9, e103750.
- [33] Coluccio, M.; Gentile, F.; Francardi, M.; Perozziello, G.; Malara, N.; Candeloro, P.; Fabrizio, E. D. Electroless Deposition and Nanolithography Can Control the Formation of Materials at the Nano-Scale for Plasmonic Applications. *Sensors* **2014**, 14, 6056–6083.
- [34] Chen, J.; Qin, G.; Chen, Q.; Yu, J.; Li, S.; Cao, F.; Yang, B.; Ren, Y. A synergistic combination of diatomaceous earth with Au nanoparticles as a periodically ordered, button-like substrate for SERS analysis of the chemical composition of eccrine sweat in latent fingerprints. *Journal of Materials Chemistry C* **2015**, 3, 4933–4944.

- [35] Lin, K.-C.; Kunduru, V.; Bothara, M.; Rege, K.; Prasad, S.; Ramakrishna, B. Biogenic nanoporous silica-based sensor for enhanced electrochemical detection of cardiovascular biomarkers proteins. *Biosensors and Bioelectronics* **2010**, *25*, 2336–2342.
- [36] Tommasi, E. D. Light Manipulation by Single Cells: The Case of Diatoms. *Journal of Spectroscopy* **2016**, *2016*, 1–13.
- [37] Brzozowska, W.; Sprynskyy, M.; Wojtczak, I.; Dąbek, P.; Witkowski, A.; Buszewski, B. “Outsourcing” Diatoms in Fabrication of Metal-Doped 3D Biosilica. *Materials* **2020**, *13*, 2576.
- [38] Nolan, J. P.; Sebba, D. S. *Methods in Cell Biology*; Elsevier, 2011; pp 515–532.
- [39] Surface-Enhanced Raman Spectroscopy Sensors From Nanobiosilica With Self-Assembled Plasmonic Nanoparticles. *IEEE Journal of Selected Topics in Quantum Electronics* **2014**, *20*, 127–132.
- [40] Kwon, S. Y.; Park, S.; Nichols, W. T. Self-assembled diatom substrates with plasmonic functionality. *Journal of the Korean Physical Society* **2014**, *64*, 1179–1184.
- [41] Wang, M.; Marepally, S.; Vemula, P.; Xu, C. *Nanoscience in Dermatology*; Elsevier, 2016; pp 57–72.
- [42] Sweet, M.; Singleton, I. *Advances in Applied Microbiology*; Elsevier, 2011; pp 115–133.
- [43] Rai, M.; Yadav, A.; Gade, A. Silver nanoparticles as a new generation of antimicrobials. *Biotechnology Advances* **2009**, *27*, 76–83.
- [44] Cobley, C. M.; Skrabalak, S. E.; Campbell, D. J.; Xia, Y. Shape-Controlled Synthesis of Silver Nanoparticles for Plasmonic and Sensing Applications. *Plasmonics* **2009**, *4*, 171–179.
- [45] Gao, J.; Fu, J.; Lin, C.; Lin, J.; Han, Y.; Yu, X.; Pan, C. Formation and Photoluminescence of Silver Nanoparticles Stabilized by a Two-Armed Polymer with a Crown Ether Core. *Langmuir* **2004**, *20*, 9775–9779.
- [46] Venkatesham, M.; Ayodhya, D.; Madhusudhan, A.; Kumari, A. S.; Veerabhadram, G.; Mangatayaru, K. G. A Novel Green Synthesis of Silver Nanoparticles Using Gum Karaya: Characterization, Antimicrobial and Catalytic Activity Studies. *Journal of Cluster Science* **2013**, *25*, 409–422.
- [47] Pattabi, M.; Pattabi, R. M. Photoluminescence from Gold and Silver Nanoparticles. *Nano Hybrids* **2014**, *6*, 1–35.

- [48] Samberg, M. E.; Oldenburg, S. J.; Monteiro-Riviere, N. A. Evaluation of Silver Nanoparticle Toxicity in Skin in Vivo and Keratinocytes in Vitro. *Environmental Health Perspectives* **2010**, *118*, 407–413.
- [49] Ali, D.; Alkahtani, S.; Gurabi, M. A. A.; Alarifi, S. In vivo DNA damaging and apoptotic potential of silver nanoparticles in Swiss albino mice. *Oncotargets and Therapy* **2015**, 295.
- [50] Montazer, M.; Harifi, T. *Nanofinishing of Textile Materials*; Elsevier, 2018; pp 19–34.
- [51] Amina, S. J.; Guo, B. A Review on the Synthesis and Functionalization of Gold Nanoparticles as a Drug Delivery Vehicle/p. *International Journal of Nanomedicine* **2020**, *Volume 15*, 9823–9857.
- [52] Su, S.; Zou, M.; Zhao, H.; Yuan, C.; Xu, Y.; Zhang, C.; Wang, L.; Fan, C.; Wang, L. Shape-controlled gold nanoparticles supported on MoS<sub>2</sub>nanosheets: synergistic effect of thionine and MoS<sub>2</sub>and their application for electrochemical label-free immunosensing. *Nanoscale* **2015**, *7*, 19129–19135.
- [53] Pissuwan, D. *Monitoring and Evaluation of Biomaterials and their Performance In Vivo*; Elsevier, 2017; pp 135–149.
- [54] Huang, X.; Jain, P. K.; El-Sayed, I. H.; El-Sayed, M. A. Gold nanoparticles: interesting optical properties and recent applications in cancer diagnostics and therapy. *Nanomedicine* **2007**, *2*, 681–693.
- [55] Pissuwan, D.; Cortie, C.; Valenzuela, S.; Cortie, M. Gold nanosphere-antibody conjugates for hyperthermal therapeutic applications. *Gold Bulletin* **2007**, *40*, 121–129.
- [56] Chen, Y.-S.; Hung, Y.-C.; Liau, I.; Huang, G. S. Assessment of the In Vivo Toxicity of Gold Nanoparticles. *Nanoscale Research Letters* **2009**, *4*, 858–864.
- [57] Grant, S. A.; Spradling, C. S.; Grant, D. N.; Fox, D. B.; Jimenez, L.; Grant, D. A.; Rone, R. J. Assessment of the biocompatibility and stability of a gold nanoparticle collagen bioscaffold. *Journal of Biomedical Materials Research Part A* **2013**, *102*, 332–339.
- [58] Shukla, R.; Bansal, V.; Chaudhary, M.; Basu, A.; Bhone, R. R.; Sastry, M. Biocompatibility of Gold Nanoparticles and Their Endocytotic Fate Inside the Cellular Compartment: A Microscopic Overview. *Langmuir* **2005**, *21*, 10644–10654.
- [59] Rosa, G. D.; Vona, D.; Aloisi, A.; Ragni, R.; Corato, R. D.; Presti, M. L.; Cicco, S. R.; Altamura, E.; Taurino, A.; Catalano, M.; Farinola, G. M.; Rinaldi, R. Luminescent Silica-Based Nanostructures from in Vivo Iridium-Doped Diatoms Microalgae. *ACS Sustainable Chemistry & Engineering* **2018**, *7*, 2207–2215.

- [60] Gale, D. K.; Jeffryes, C.; Gutu, T.; Jiao, J.; hung Chang, C.; Rorrer, G. L. Thermal annealing activates amplified photoluminescence of germanium metabolically doped in diatom biosilica. *Journal of Materials Chemistry* **2011**, *21*, 10658.
- [61] Pannico, M.; Rea, I.; Chandrasekaran, S.; Musto, P.; Voelcker, N. H.; Stefano, L. D. Electroless Gold-Modified Diatoms as Surface-Enhanced Raman Scattering Supports. *Nanoscale Research Letters* **2016**, *11*.
- [62] Kamińska, A.; Sprynskyy, M.; Winkler, K.; Szymborski, T. Ultrasensitive SERS immunoassay based on diatom biosilica for detection of interleukins in blood plasma. *Analytical and Bioanalytical Chemistry* **2017**, *409*, 6337–6347.
- [63] Chamuah, N.; Chetia, L.; Zahan, N.; Dutta, S.; Ahmed, G. A.; Nath, P. A naturally occurring diatom frustule as a SERS substrate for the detection and quantification of chemicals. *Journal of Physics D: Applied Physics* **2017**, *50*, 175103.
- [64] Khurana, K.; Jaggi, N. Localized Surface Plasmonic Properties of Au and Ag Nanoparticles for Sensors: a Review. *Plasmonics* **2021**,
- [65] Cai, J.; Wang, Z.; Wang, M.; Zhang, D. Au nanoparticle-grafted hierarchical pillars array replicated from diatom as reliable SERS substrates. *Applied Surface Science* **2021**, *541*, 148374.
- [66] Chang, S.; Combs, Z. A.; Gupta, M. K.; Davis, R.; Tsukruk, V. V. In situ Growth of Silver Nanoparticles in Porous Membranes for Surface-Enhanced Raman Scattering. *ACS Applied Materials & Interfaces* **2010**, *2*, 3333–3339.
- [67] Kong, X.; Squire, K.; Li, E.; LeDuff, P.; Rorrer, G. L.; Tang, S.; Chen, B.; McKay, C. P.; Navarro-Gonzalez, R.; Wang, A. X. Chemical and Biological Sensing Using Diatom Photonic Crystal Biosilica With In-Situ Growth Plasmonic Nanoparticles. *IEEE Transactions on NanoBioscience* **2016**, *15*, 828–834.
- [68] Bose, R.; Roychoudhury, P.; Pal, R. In-situ green synthesis of fluorescent silica–silver conjugate nanodendrites using nanoporous frustules of diatoms: an unprecedented approach. *Bioprocess and Biosystems Engineering* **2021**,
- [69] Larkin, P. *Infrared and Raman Spectroscopy*; Elsevier, 2011; pp 1–5.
- [70] Colthup, N. *Introduction to Infrared and Raman Spectroscopy*; Elsevier Science, 2012.

- [71] Chen, W.; Wang, J.; Wan, F.; Wang, P. Review of optical fibre sensors for electrical equipment characteristic state parameters detection. *High Voltage* **2019**, *4*, 271–281.
- [72] Krull, U. J.; Thompson, M. *Encyclopedia of Physical Science and Technology*; Elsevier, 2003; pp 543–579.
- [73] Rostron, P.; Gerber, D. Raman Spectroscopy, a review. *International Journal of Engineering and Technical Research* **2016**, *6*, 50–64.
- [74] Raja, P. M. V.; Barron, A. R. Raman Spectroscopy. 2021; <https://chem.libretexts.org/@go/page/55879>, [Online; accessed 2021-05-22].
- [75] Bumbrah, G. S.; Sharma, R. M. Raman spectroscopy – Basic principle, instrumentation and selected applications for the characterization of drugs of abuse. *Egyptian Journal of Forensic Sciences* **2016**, *6*, 209–215.
- [76] Ru, E. C. L.; Etchegoin, P. G. *Principles of Surface-Enhanced Raman Spectroscopy*; Elsevier, 2009; pp 1–27.
- [77] *Principles of Surface-Enhanced Raman Spectroscopy*; Elsevier, 2009.
- [78] Bora, T. *Noble and Precious Metals - Properties, Nanoscale Effects and Applications*; InTech, 2018.
- [79] Chen, Z.; Deutsch, T. G.; Dinh, H. N.; Domen, K.; Emery, K.; Forman, A. J.; Gaillard, N.; Garland, R.; Heske, C.; Jaramillo, T. F.; Kleiman-Shwarsstein, A.; Miller, E.; Takanabe, K.; Turner, J. *SpringerBriefs in Energy*; Springer New York, 2013; pp 49–62.
- [80] Omidi, M.; Fatehinya, A.; Farahani, M.; Akbari, Z.; Shahmoradi, S.; Yazdian, F.; Tahriri, M.; Moharamzadeh, K.; Tayebi, L.; Vashae, D. *Biomaterials for Oral and Dental Tissue Engineering*; Elsevier, 2017; pp 97–115.
- [81] Inkson, B. *Materials Characterization Using Nondestructive Evaluation (NDE) Methods*; Elsevier, 2016; pp 17–43.
- [82] Echlin, P. *Handbook of Sample Preparation for Scanning Electron Microscopy and X-Ray Microanalysis*; Springer US, 2009.
- [83] Wen, Y.; Shang, T.; Gu, L. Analytical ABF-STEM imaging of Li ions in rechargeable batteries. *Microscopy (Oxford, England)* **2016**, *66*.
- [84] Singh, A. K. *Engineered Nanoparticles*; Elsevier, 2016; pp 125–170.

- [85] García-Negrete, C. A.; de Haro, M. C. J.; Blasco, J.; Soto, M.; Fernández, A. STEM-in-SEM high resolution imaging of gold nanoparticles and bivalve tissues in bioaccumulation experiments. *The Analyst* **2015**, *140*, 3082–3089.
- [86] Wall, J. S.; Simon, M. N.; Lin, B. Y.; Vinogradov, S. N. *Methods in Enzymology*; Elsevier, 2008; pp 487–501.
- [87] Muller, D. A.; Kirkland, E. J.; Thomas, M. G.; Grazul, J. L.; Fitting, L.; Weyland, M. Room design for high-performance electron microscopy. *Ultramicroscopy* **2006**, *106*, 1033–1040.
- [88] Rost, F. *Encyclopedia of Spectroscopy and Spectrometry*; Elsevier, 2017; pp 627–631.
- [89] Titus, D.; Samuel, E. J. J.; Roopan, S. M. *Green Synthesis, Characterization and Applications of Nanoparticles*; Elsevier, 2019; pp 303–319.
- [90] Mohamed, M.; Jaafar, J.; Ismail, A.; Othman, M.; Rahman, M. *Membrane Characterization*; Elsevier, 2017; pp 3–29.
- [91] Saade, J.; de Araújo, C. B. Synthesis of silver nanoprisms: A photochemical approach using light emission diodes. *Materials Chemistry and Physics* **2014**, *148*, 1184–1193.
- [92] Kim, D.-Y.; Kim, M.; Shinde, S.; Saratale, R. G.; Sung, J.-S.; Ghodake, G. Temperature Dependent Synthesis of Tryptophan-Functionalized Gold Nanoparticles and Their Application in Imaging Human Neuronal Cells. *ACS Sustainable Chemistry & Engineering* **2017**, *5*, 7678–7689.
- [93] Gupta, S.; Kashyap, M.; Kumar, V.; Jain, P.; Vinayak, V.; Joshi, K. B. Peptide mediated facile fabrication of silver nanoparticles over living diatom surface and its application. *Journal of Molecular Liquids* **2018**, *249*, 600–608.
- [94] Chetia, L.; Kalita, D.; Ahmed, G. A. Synthesis of Ag nanoparticles using diatom cells for ammonia sensing. *Sensing and Bio-Sensing Research* **2017**, *16*, 55–61.
- [95] Cai, Y.; Piao, X.; Gao, W.; Zhang, Z.; Nie, E.; Sun, Z. Large-scale and facile synthesis of silver nanoparticles via a microwave method for a conductive pen. *RSC Advances* **2017**, *7*, 34041–34048.
- [96] Meksjarun, P.; Spegazzini, N.; Matsui, H.; Nakajima, K.; Matsuda, Y.; Sato, H. In Vivo Study of Lipid Accumulation in the Microalgae Marine Diatom *Thalassiosira pseudonana* Using Raman Spectroscopy. *Applied Spectroscopy* **2015**, *69*, 45–51.

- [97] Pudlarz, A. M.; Ranoszek-Soliwoda, K.; Czechowska, E.; Tomaszewska, E.; Celichowski, G.; Grobelny, J.; Szemraj, J. A Study of the Activity of Recombinant Mn-Superoxide Dismutase in the Presence of Gold and Silver Nanoparticles. *Applied Biochemistry and Biotechnology* **2018**, *187*, 1551–1568.
- [98] Villani, M.; Onesto, V.; Coluccio, M.; Valpapuram, I.; Majewska, R.; Alabastri, A.; Battista, E.; Schirato, A.; Calestani, D.; Coppedé, N.; Zappettini, A.; Amato, F.; Fabrizio, E. D.; Gentile, F. Transforming diatomaceous earth into sensing devices by surface modification with gold nanoparticles. *Micro and Nano Engineering* **2019**, *2*, 29–34.
- [99] Taboury, J. A.; Liquier, J.; Taillandier, E. Characterization of DNA structures by infrared spectroscopy: double helical forms of poly(dG-dC)•poly(dG-dC), poly(dD8G-dC)•poly(dD8G-dC), and poly(dG-dm5C)•poly(dG-dm5C). *Canadian Journal of Chemistry* **1985**, *63*, 1904–1909.
- [100] Alipour, L.; Hamamoto, M.; Nakashima, S.; Harui, R.; Furiki, M.; Oku, O. Infrared Microspectroscopy of Bionanomaterials (Diatoms) with Careful Evaluation of Void Effects. *Applied Spectroscopy* **2016**, *70*, 427–442.
- [101] Saini, R. K.; Keum, Y.-S. Carotenoid extraction methods: A review of recent developments. *Food Chemistry* **2018**, *240*, 90–103.
- [102] Cahoon, L.; Halkides, C.; Song, B.; Williams, C.; Dubay, G.; Fries, A.; Farmer, J.; Fridrich, W.; Brookshire, C. Swine waste as a source of natural products: A carotenoid antioxidant. *Agricultural Sciences* **2012**, *3*, 806–815.
- [103] der Horst, C. V.; Silwana, B.; Iwuoha, E.; Somerset, V. Synthesis and Characterization of Bismuth-Silver Nanoparticles for Electrochemical Sensor Applications. *Analytical Letters* **2014**, *48*, 1311–1332.
- [104] Ramirez, D. E.; Jaramillo, F. Fácil síntesis en un paso y mecanismo de formación de nanopartículas de plata. *DYNA* **2016**, *83*, 165.
- [105] Mazumder, N.; Gogoi, A.; Buragohain, A. K.; Ahmed, G. A.; Choudhury, A. Structural and optical characterization of fresh water diatoms (*Cyclotella* sp.): nature's nanoporous silica manufacturing plant. 2014; <https://doi.org/10.1117/12.2039793>.
- [106] Wieneke, R.; Bernecker, A.; Riedel, R.; Sumper, M.; Steinem, C.; Geyer, A. Silica precipitation with synthetic silaffin peptides. *Organic & Biomolecular Chemistry* **2011**, *9*, 5482.

- [107] Gale, D. K.; Gutu, T.; Jiao, J.; Chang, C.-H.; Rorrer, G. L. Photoluminescence Detection of Biomolecules by Antibody-Functionalized Diatom Biosilica. *Advanced Functional Materials* **2009**, *19*, 926–933.